Pseudoratchet through one-dimensional quantum Brownian motion for energy-efficient Brownian computing

Sho Nakade [1,2,*] Ferdinand Peper,[1,†] Kazuki Kanki [3,‡] and Tomio Petrosky [4,5,§]

[1]*Advanced ICT Research Institute, National Institute of Information and Communications Technology, Iwaoka 588-2, Kobe 651-2401, Japan*

[2]*Department of Electrical and Electronics Engineering, Mie University, 1577, Kurimamachiya-cho, Tsu 514-8507, Japan*

[3]*Department of Physics and Nambu Yoichiro Institute of Theoretical and Experimental Physics (NITEP), Osaka Metropolitan University, 3-3-138 Sugimoto, Sumiyoshi-ku, Osaka 558-8585, Japan*

[4]*Center for Complex Quantum Systems, The University of Texas at Austin, Austin, Texas 78712, USA*

[5]*Institute of Industrial Science, The University of Tokyo, 5-1-5, Kashiwa 277-851, Japan*

(Received 13 May 2025; accepted 23 November 2025; published 19 December 2025)

We propose a pseudoratchet mechanism based on one-dimensional (1D) quantum Brownian motion, offering a route to energy-efficient Brownian computing without relying on conventional ratchet structures. Quantum resonance effects in 1D system naturally partition the momentum space into dynamically independent subspaces, each of which lacks inversion symmetry. This leads to spontaneous unidirectional particle transport near thermal equilibrium, without external forces or asymmetric potential gradients. We analyze this pseudoratchet mechanism from kinetic and entropic perspectives and show that the directional transport is sustained without energy dissipation, remaining fully consistent with the second law of thermodynamics. Our analysis provides a microscopic and physically grounded foundation for reversible information transport in Brownian computing.

DOI: 10.1103/fskm-y179

I. INTRODUCTION

In the quest for ultra-low-energy computing, there has been growing interest in utilizing thermal fluctuations near equilibrium as computational resources, leading to the concept of "Brownian computing" [1]. Since Brownian motion maintains a momentum distribution in Maxwell-Boltzmann equilibrium, energy dissipation associated with momentum relaxation can be avoided. Furthermore, because the computation can proceed spontaneously through thermal fluctuations, when combined with logically reversible computation [2–5] that does not involve information erasure, it is theoretically possible to approach vanishingly small energy dissipation [1,6,7].

As a concrete architecture for Brownian computing, *Brownian circuits* that use Brownian particles as signal carriers have been proposed [8–10]. This architecture consists of two types of gate elements connected by wires, where signals—realized as particles called *tokens*—undergo Brownian motion along the circuits' [one-dimensional (1D)] wires, enabling universal computation in principle. Physical implementations have been explored in single-electron tunneling circuits [10–12], skyrmion-based circuits [13,14], and single-flux-quantum circuits [15].

Within this framework, information is physically encoded in the position of a Brownian particle (token), meaning that the final computational outcome is determined by the particle's arrival at the corresponding designated target position. However, because classical Brownian motion is inherently directionless, it can take an extremely long time for the particle to reach this position [1,7]. More fundamentally, in the absence of external intervention, a Brownian particle cannot deterministically reach the target position as its motion is inherently stochastic, making precise and reliable completion of the computation physically unattainable [16,17]. This is a well-known consequence of continuous-time Markov processes, in which certain computational operations, such as enforcing a deterministic state transition within a finite time, are fundamentally unimplementable [18].

These challenges have been addressed in Refs. [9,16,17,19] by introducing external manipulation in Brownian computers. One approach [8–10] involves using a device called *ratchet* that restricts particle motion to a single direction. By transporting particles in a unidirectional manner, the device not only shortens the computation time but also reduces the uncertainty in arrival time at the target position [20]. Consequently, this reduction in arrival time uncertainty enhances the reliability of computation and can mitigate the cost of measurement required for confirming computation completion by reducing the measurement frequency.

However, inducing the directed motion of a Brownian particle requires work to be performed on the particle and thus entails energy dissipation [21]. Therefore, both improving

*Contact author: shonakade.lab@gmail.com
†Contact author: peper@nict.go.jp
‡Contact author: kanki@omu.ac.jp
§Contact author: petrosky@austin.utexas.edu

computation speed and enhancing reliability of computation involve fundamental trade-offs with minimizing energy consumption [22,23].

Directional Brownian motion is typically described by an advection-diffusion equation (i.e., the Fokker-Planck equation in the overdamped regime) [24]. The advection term describes the unidirectional motion induced by an external force or a potential, and necessarily involves energy input and dissipation.

The classical Brownian ratchet [25–28] is also described by an advection-diffusion equation, where the advection term arises from an asymmetric periodic potential combined with a time-periodic external field. In this framework, the external field does not perform net work on the particle. However, the time-periodic driving maintains the system in a nonequilibrium state, which inherently leads to entropy production and heat dissipation. As a result, the ratchet effect cannot be sustained unless energy is continuously supplied.

In this paper, we propose an approach to overcome these limitations by employing Brownian motion in a 1D quantum system. The key advantage lies in the one-dimensionality and quantum nature of the system. The particle in our model, remarkably, obeys an advection-diffusion equation even in the absence of any external forces or potential gradients [29]:

$$\frac{\partial}{\partial t} f^W(X,P,t) = -\sigma(P)\frac{\partial}{\partial X} f^W(X,P,t) + D(P)\frac{\partial^2}{\partial X^2} f^W(X,P,t), \quad (1)$$

where $f^W(X,P,t)$ is the Wigner distribution function of the particle. The first term on the right-hand side represents the advection, describing unidirectional transport with the hydrodynamic sound velocity $\sigma(P)$. The second term corresponds to the diffusion process, spreading the distribution with the diffusion coefficient $D(P)$. Both transport coefficients, $\sigma(P)$ and $D(P)$, depend on momentum.

As a result, this system realizes ratchetlike behavior without conventional energy dissipation mechanisms. Consequently, our 1D quantum system opens up the possibility of mitigating the trade-off between computation efficiency (speed and reliability) and energy dissipation that has long been considered inevitable in classical Brownian computing.

However, when Brownian particles can be transported in one direction without external manipulation, a question of consistency with the second law of thermodynamics arises, which has been discussed in the context of the Feynman ratchet [30] and Maxwell's demon [31,32]. In fact, in our previous paper [33], we showed that in this one-dimensional quantum system, depending on the initial conditions, the phenomenologically defined diffusion coefficient can take negative values, leading to a spontaneous contraction of the spatial distribution. Nevertheless, we also proved that the H theorem holds in this system, ensuring no violation of the second law of thermodynamics.

The main purpose of this paper is not to present a practical implementation of Brownian computers, but rather to establish their theoretical physical foundations by clarifying the microscopic thermodynamic consistency in this system. To this end, we identify specific initial conditions under which the spatial distribution contracts and analyze the underlying mechanism in terms of the relative entropy (also known as the Kullback-Leibler divergence [37]) associated with the correlation between coordinate and momentum. Our key finding is that, in this 1D quantum system, a nonzero relative entropy provides the microscopic basis for both the emergence of unidirectional transport via the advection term—without violating the second law of thermodynamics or requiring external control—and, in some cases, the contraction of the spatial distribution.

Our model considers a quantum particle weakly coupled to 1D lattice vibrations, which form a quantized phonon field acting as a thermal reservoir. Under the stringent spatial confinement of a 1D system, phonon scattering restricts the set of accessible momentum states, partitioning the particle's momentum space into disjoint subspaces [34,35]. Since these subspaces lack momentum inversion symmetry, the equilibrium momentum distribution established within each subspace becomes asymmetric, resulting in a nonzero average velocity and thus unidirectional transport [29].

As we will discuss in detail in this paper, our primary finding is that, due to the partitioning of the particle's momentum space into disjoint subspaces, an initial correlation between coordinates and momenta—quantified by the relative entropy—remains even after the momentum distribution has relaxed to a local equilibrium state. This persistence indicates that the transport direction of Brownian particles at a given coordinate can be controlled by appropriately choosing the initial conditions.

Crucially, in this 1D setting, dissipation is purely a quantum effect. If the phonon field is treated in the classical limit, the collision terms vanish, and no dissipation occurs in the one-dimensional classical regime [34]. This is because, under the extreme confinement of one dimension, the resonance conditions required for momentum exchange via particle-phonon interactions are severely restricted and cannot be fulfilled classically. In contrast, in a quantum system, the particle can undergo momentum transitions by absorbing or emitting quantized phonons, thereby leading to dissipation.

It should be emphasized that the partitioning of the momentum space, which is a manifestation of the 1D quantum dissipation effect, is independent of temperature. This is because the partitioning stems from the resonance condition in the collision operator and this condition itself is temperature independent. This implies that the ratchetlike behavior analyzed in this paper can remain effective over a wide range of temperatures.

Our approach is grounded in microscopic kinetic theory [36], enabling us to derive the particle's advection-diffusion equation in the hydrodynamic regime and to analyze its dynamics in detail. This approach is crucial because it allows us to relate transport coefficients, which are often introduced phenomenologically, to underlying microscopic principles.

Since the main purpose of this paper is to focus on the role of relative entropy, we will only list the detailed properties and formulas of the above advection-diffusion equation (1) necessary for this discussion without proof. The detailed microscopic derivations can be found in Refs. [29,34].

This paper is organized as follows. In Sec. II, we explain the mechanism underlying the emergence of unidirectional

transport from the perspective of kinetic theory. In Sec. III, we introduce an initial state that leads to the contraction of the spatial distribution and analyze the contraction by examining the time evolution of the mean-square displacement. In Sec. IV, we discuss the central issue of this paper. Here, we explain this spatial contraction scenario from an entropic perspective using relative entropy. Finally, Sec. V summarizes our results and their potential implications for the practical realization of Brownian computers. In addition, Appendix B illustrates where the pseudoratchet effect could be exploited within Brownian circuits.

II. MECHANISM OF UNIDIRECTIONAL TRANSPORT WITHOUT EXTERNAL FORCES

In this section, we explain the microscopic mechanism behind the unidirectional transport of 1D quantum Brownian particle from kinetic perspective and summarize its transport properties. The key origin of all the peculiar phenomena discussed in this paper is the partitioning of momentum space into subspaces, which arises from the resonance condition of collision operator in the 1D quantum system. Detailed analyses and derivations are available in Refs. [29,34].

A. Model and kinetic equation

The model under consideration describes a quantum particle coupled to phonons in a 1D lattice. This model is known as the Davydov Hamiltonian [34,39,40] in the context of biological systems, where it describes a vibrational exciton weakly coupled to acoustic phonons of underlying lattice along a 1D α-helical protein molecular chain. The same model and its interaction mechanism [Eq. (6)], referred to as the deformation-potential interaction, are also widely used in semiconductor physics to describe the coupling between a free electron and acoustic phonons [41].

The Hamiltonian of this model is given by

$$H = H_0 + gV, \tag{2}$$

$$H_0 = \sum_p \varepsilon_p |p\rangle\langle p| + \sum_q \hbar\omega_q a_q^\dagger a_q, \tag{3}$$

$$gV = \sqrt{\frac{2\pi}{L}} \sum_{p,q} gV_q |p+\hbar q\rangle\langle p|(a_q + a_{-q}^\dagger), \tag{4}$$

where the dispersion relations and interaction potential take the following forms:

$$\varepsilon_p = \frac{p^2}{2m}, \qquad \omega_q = c|q|, \tag{5}$$

$$gV_q = g\Delta_0 |q| \sqrt{\frac{\hbar}{4\pi\rho_M\omega_q}}. \tag{6}$$

Here, $|p\rangle$ denotes the momentum state of the particle, orthonormalized by the Kronecker delta, $a_q^\dagger$ and a_q are phonon creation and annihilation operators with wave number q, respectively, and L is the length of the system. We consider the case $L \gg d$, where d is the lattice constant of the 1D molecular chain. Thus, we will consider the case $L/d \to \infty$, and we will shift from the Kronecker delta normalization to the delta function normalization in an appropriate stage of the calculations. The parameter m denotes the effective mass of the particle, c is the propagation speed of acoustic phonons in the 1D system, ρ_M is the mass density of the system, and $g\Delta_0$ is the coupling constant, where g is a dimensionless coupling constant used to indicate the order of the perturbation expansion and is set to 1 after the weak-coupling approximation.

We consider the time evolution of the reduced density operator for the particle, $f(t) := \mathrm{Tr}_{\mathrm{ph}}[\rho(t)]$, where $\mathrm{Tr}_{\mathrm{ph}}$ represents the trace over all phonon modes. We assume that the phonons are in thermal equilibrium at temperature T.

Using Dirac's bra-ket notations ($p|$ and $|p'$) for the momentum states, we introduce the Wigner basis [38,42] as the representation basis for the reduced density operator $f(t)$: $f_k(P,t) := (P + \hbar k/2|f(t)|P - \hbar k/2)$. Here, the round bracket is normalized by the Dirac delta function $(p|p') = \delta(p - p')$.

The Fourier transform of $f_k(P,t)$ with respect to k defines the Wigner distribution function in "phase space":

$$f^W(X,P,t) := \frac{1}{2\pi}\int_{-\infty}^{\infty} dk\, e^{ikX} f_k(P,t). \tag{7}$$

Note that the $k = 0$ component, $f_0(P,t)$, corresponds to the momentum distribution, while the $k \neq 0$ components represent spatial inhomogeneities.

In the weak coupling approximation, $f_k(P,t)$ obeys the Markovian kinetic equation [38,42,43],

$$\frac{\partial}{\partial t} f_k(P,t) = \mathcal{K}_P^{(k)} f_k(P,t), \tag{8}$$

with the collision operator given by

$$\mathcal{K}_P^{(k)} = -ik\frac{P}{m} + \mathcal{K}_P^{(0)}, \tag{9}$$

where the first term represents the time-reversible flow term and the second term represents the irreversible collision term, which governs the momentum relaxation. The explicit form of the collision term in the second-order approximation is given by [34]

$$\begin{aligned}\mathcal{K}_P^{(0)} = {} & g^2\frac{2\pi}{\hbar^2}\int dq|V_q|^2\delta\left(\frac{\varepsilon_{P-\hbar q} - \varepsilon_P}{\hbar} + \omega_q\right) n(q) e^{-\hbar q\frac{\partial}{\partial P}} \\ & + g^2\frac{2\pi}{\hbar^2}\int dq|V_q|^2\delta\left(\frac{\varepsilon_P - \varepsilon_{P+\hbar q}}{\hbar} + \omega_q\right)(n(q)+1) e^{\hbar q\frac{\partial}{\partial P}} \\ & - g^2\frac{2\pi}{\hbar^2}\int dq|V_q|^2\delta\left(\frac{\varepsilon_P - \varepsilon_{P+\hbar q}}{\hbar} + \omega_q\right) n(q) \\ & - g^2\frac{2\pi}{\hbar^2}\int dq|V_q|^2\delta\left(\frac{\varepsilon_{P-\hbar q} - \varepsilon_P}{\hbar} + \omega_q\right)(n(q)+1),\end{aligned} \tag{10}$$

where $n(q)$ is the average number of phonons with wave number q, which follows the Bose-Einstein distribution:

$$n(q) := \frac{1}{\exp[\hbar\omega_q/k_B T] - 1}. \tag{11}$$

Reflecting the quantum nature of the system, the collision term (10) acts as a momentum-shift operator: $\exp(\pm\hbar q \cdot \partial/\partial P) f(P) = f(P \pm \hbar q)$. An important point to note is that in the classical limit of the phonon field, where Planck's constant $\hbar$ is negligible compared to the action variable J_q of

the phonon modes (i.e., $\hbar \ll J_q$), the collision term reduces to $\int dq\ q\delta(q)$ and vanishes [34]. This indicates that the dissipation in this one-dimensional weak coupling system is a purely quantum effect, arising from the quantized nature of the phonon field.

Let us define the momentum after a phonon absorption or emission as $P' = P \pm \hbar q$. The resonance condition is then

$$\begin{aligned} 0 &= \varepsilon_{P'} - \varepsilon_P \pm \hbar\omega_{|P'-P|/\hbar} \\ &= \frac{1}{2m}(P' - P)(P' + P \pm 2mc \cdot \mathrm{sgn}(P' - P)), \end{aligned} \tag{12}$$

where $\mathrm{sgn}(\cdot)$ is a sign function, defined as $\mathrm{sgn}(x) = +1$ if $x > 0$, -1 if $x < 0$, and 0 if $x = 0$. This indicates that the only allowed momentum transitions from state P are two states $P' = -P \pm 2mc$. Starting from an initial momentum P_0, all the momenta successively connected by the collision term are enumerated in the form of a recurrence relation for integer ν:

$$P_{\nu\pm1} = -P_\nu \pm (-1)^\nu 2mc \tag{13}$$

[see Fig. 9(a)]. Note that, since Eq. (12) is temperature independent, the subspace structure in 1D persists at all temperatures.

B. Partitioning of momentum space and asymmetric Maxwellian distribution

A key feature of this system is that the resonance condition constrains the particle's momentum transitions via phonon absorption or emission. As a result, starting from an initial momentum P_0, all the momenta that are successively connected through the collision process form a discrete set:

$$P_\nu = (-1)^\nu (P_0 - 2\nu mc), \quad (\nu = 0, \pm1, \pm2, \ldots). \tag{14}$$

To label each of these sets uniquely and avoid overlaps, we restrict P_0 to the range

$$-mc \leqslant P_0 \leqslant mc \tag{15}$$

and denote the corresponding momentum subspace by $\mathcal{S}_{P_0}$. Each subspace $\mathcal{S}_{P_0}$ is closed under the resonance condition.

Because the momentum relaxation occurs within each $\mathcal{S}_{P_0}$, the equilibrium distribution corresponding to a zero eigenfunction of the collision operator (i.e., a collisional invariant associated with particle number) is given by

$$\varphi^{\mathrm{eq}}_{P_0}(P_\nu) = \frac{\exp\left[-\varepsilon_{P_\nu(P_0)}/k_\mathrm{B}T\right]}{\sum_{\mu=-\infty}^{\infty}\exp\left[-\varepsilon_{P_\mu(P_0)}/k_\mathrm{B}T\right]}, \tag{16}$$

where the notation $P_\nu(P_0)$ emphasizes its dependence on P_0.

The Maxwellian distribution (16) is asymmetric when $P_0 \neq 0$. This is because, for $P_0 \neq 0$, the subspace $\mathcal{S}_{P_0}$ itself lacks inversion symmetry. Specifically, applying the inversion operation $P \mapsto -P$ to a discrete momentum in $\mathcal{S}_{P_0}$ yields a momentum that does not belong to the same subspace:

$$P_\nu(P_0) \xrightarrow{P\mapsto -P} -P_\nu(P_0) \notin \mathcal{S}_{P_0}, \quad (\forall P_0 \neq 0). \tag{17}$$

Instead, the inverted momentum corresponds to the $-\nu$th discrete momentum in the subspace $\mathcal{S}_{-P_0}$:

$$-P_\nu(P_0) = P_{-\nu}(-P_0) \in \mathcal{S}_{-P_0}, \quad (\forall P_0 \neq 0). \tag{18}$$

Thus, each subspace $\mathcal{S}_{P_0}$ has a mirror counterpart $\mathcal{S}_{-P_0}$, so that momentum inversion symmetry is preserved when the entire momentum space is considered.

In systems with two or more dimensions, the resonance condition allows infinitely many momentum transitions due to angular degrees of freedom, and no partitioning of momentum space occurs. Consequently, the equilibrium distribution in higher dimensions has momentum inversion symmetry.

C. Transport properties in the hydrodynamic regime

We summarize the transport properties of the 1D quantum Brownian particle in the hydrodynamic regime, where the spatial variation of the particle distribution is characterized by long wavelengths, i.e., small wave number k.

Since relaxation dynamics occur within each subspace, different transport modes emerge for each subspace. Specifically, in the hydrodynamic regime, after the momentum relaxation time τ_{rel}, the Wigner distribution function (7) for the reduced density matrix of the particle with a momentum P_ν belonging to a subspace $\mathcal{S}_{P_0}$ behaves [29] as follows:

$$f^W(X, P_\nu, t \gtrsim \tau_{\mathrm{rel}}) \simeq \chi_{P_0}(X, t)\varphi^{\mathrm{eq}}_{P_0}(P_\nu), \tag{19}$$

where

$$\begin{aligned} \chi_{P_0}(X, t) := \frac{1}{2\pi}\int_{-\infty}^{\infty} dk\ e^{ik\{X - \sigma(P_0)t\}} e^{-k^2 D(P_0)t} \\ \times \sum_{\mu=-\infty}^{\infty} f_k(P_\mu(P_0), 0). \end{aligned} \tag{20}$$

Here, $\sigma(P_0)$ and $D(P_0)$ represent the hydrodynamic sound velocity and diffusion coefficient, respectively, within the subspace $\mathcal{S}_{P_0}$.

Equation (19) is valid under local equilibrium, where the momentum distribution within each subspace has already relaxed to the Maxwellian (16). At this stage, spatial relaxation is still in progress, governed by the small perturbation (approximated up to the second order in k) to the zero eigenvalue of the collision term. Note that because $\chi_{P_0}(X, t)$ depends on P_0, the Wigner distribution function cannot be separated into functions of X and of P, even after momentum relaxation.

The hydrodynamic sound velocity $\sigma(P_0)$ takes the form of the average velocity of the particle in the momentum equilibrium state within the subspace $\mathcal{S}_{P_0}$:

$$\sigma(P_0) = \sum_{\nu=-\infty}^{\infty} \frac{P_\nu}{m}\varphi^{\mathrm{eq}}_{P_0}(P_\nu) = \frac{\sum_{\nu=-\infty}^{\infty} \frac{P_\nu}{m}\exp\left(-\frac{P_\nu^2}{2mk_\mathrm{B}T}\right)}{\sum_{\mu=-\infty}^{\infty}\exp\left(-\frac{P_\mu^2}{2mk_\mathrm{B}T}\right)}. \tag{21}$$

The lack of momentum inversion symmetry in $\mathcal{S}_{P_0}$ prevents the cancellation of ν and $-\nu$ components in the summation. Consequently, $\sigma(P_0)$ takes nonzero positive or negative values, except for the symmetric case $P_0 = 0$, where $\sigma(P_0) = 0$.

On the other hand, the diffusion coefficient $D(P_0)$ always takes positive values,

$$D(P_0) > 0. \tag{22}$$

Since these coefficients depend only on the subspace itself and not on the specific choice of the initial momentum within the

subspace, the following relations hold:

$$\sigma(P_0) = \sigma(P_\nu), \quad D(P_0) = D(P_\nu); \quad (\nu = 0, \pm 1, \pm 2, \ldots). \tag{23}$$

For detailed analyses of the transport coefficients, see Ref. [29], where the analytical expression of $\sigma(P_0)$ is given in terms of elliptic theta functions.

Since P_ν spans the entire continuous momentum space as P_0 varies over the range (15), we treat the Wigner distribution function as defined on the continuous momentum P, with integration performed via

$$\int_{-\infty}^{\infty} dP\, f^W(X, P, t) = \int_{-mc}^{mc} dP_0 \sum_{\nu=-\infty}^{\infty} f^W(X, P_\nu(P_0), t). \tag{24}$$

By differentiating Eq. (19) with respect to t and comparing the result with its spatial derivatives, we obtain the advection-diffusion equation (1).

Equation (1) is formally equivalent to the Fokker-Planck equation for overdamped systems [24], which commonly describes directional Brownian motion driven by an external force or potential gradient [24], or classical Brownian ratchet systems where the advection term arises from an asymmetric periodic potential combined with a time-periodic external field [25–28]. In such systems, directed transport requires external driving and involves energy dissipation, rendering the advection irreversible.

In contrast, our 1D quantum system naturally exhibits an advection term in Eq. (1) without external forces or potential gradients. This implies that directed transport in this system is sustained at local equilibrium without energy dissipation, and remarkably, the advection is a time-reversible effect.

Time reversibility of the advection can be shown as follows. Under time reversal $t \mapsto -t$, the momentum is reversed $P \mapsto -P$, which in turn flips the sign of the sound velocity:

$$\sigma(P) \xrightarrow{P \mapsto -P} \sigma(-P) = -\sigma(P). \tag{25}$$

This can be proven using Eqs. (18), (21), and (23).

This time reversibility indicates that the initial conditions play a crucial role in the emergence of unidirectional transport. Specifically, if the initial state $f_k(P_\mu(P_0), 0)$ in Eq. (20) has an asymmetric momentum distribution, the paired subspaces $\mathcal{S}_{P_0}$ and $\mathcal{S}_{-P_0}$ carry different weights, leading to an asymmetric equilibrium momentum distribution across the entire momentum space. As a result, the total advection, integrated over all momentum space, becomes nonzero. Conversely, if the initial state has a symmetric momentum distribution, the paired subspaces have equal weights, resulting in a symmetric momentum equilibrium distribution and, thus, zero total advection.

Since the reversible advection effect (proportional to k) allows the particle to be transported in one direction with small spreading of the distribution due to the diffusion effect (proportional to k^2), it enables nearly reversible information transport. This resembles free-particle propagation, but is realized within a dissipative environment.

Importantly, our system exhibits this advection without requiring external driving mechanisms or incurring energy costs, thereby avoiding the inevitable cost associated with conventional Brownian computing approaches. This suggests the possibility of constructing more energy-efficient Brownian computers. The explicit illustration of unidirectional transport and its potential role as a pseudoratchet in Brownian computing are provided in the Appendixes (see Appendixes A and B).

III. ADVECTION-INDUCED SPATIAL CONTRACTION IN 1D QUANTUM BROWNIAN MOTION

In the previous section, we have shown a mechanism by which a Brownian particle in the 1D quantum system follows the advection-diffusion equation without external force, and unidirectional transport is induced by the advection term. This results in a ratchetlike behavior without energy dissipation.

However, if a ratchet without energy dissipation exists, it could locally counteract diffusion. In particular, by installing two such ratchets in opposite directions, the system could lead to the contraction of the spatial distribution of the particle without paying any thermodynamic cost, which would appear to contradict the second law of thermodynamics.

In this section, we illustrate how, by setting specific initial conditions, the unidirectional transport in this 1D quantum system spontaneously leads to the contraction of the spatial distribution. Furthermore, by discussing this, we will see that for such a contraction to occur, it is essential that the correlation between particle coordinate and momentum does not disappear, and therefore the role of the relative entropy associated with that correlation becomes important, which is the central issue of this paper as mentioned in the introduction.

This phenomenon can be characterized by the phenomenologically defined diffusion coefficient, which is given by the time derivative of the mean-square displacement:

$$D^{(x)}(t) := \frac{1}{2}\frac{d}{dt}\langle (X - \langle X\rangle_t)^2\rangle_t, \tag{26}$$

where the average $\langle\cdot\rangle_t$ is taken over the Wigner distribution function $f^W(X, P, t)$.

In our model, the phenomenological diffusion coefficient $D^{(x)}(t)$ can take a negative value, meaning that the spatial distribution narrows over time, manifesting "negative diffusion." At first glance, this spatial contraction might appear to contradict the second law of thermodynamics, as it suggests a spontaneous decrease in entropy associated with the uncertainty in the position of the particle. [Specifically, the uncertainty corresponds to the width of the probability distribution. For example, consider a Gaussian distribution $N(x; \mu_X, s_X^2)$ with mean μ_X and standard deviation s_X. Its entropy is given by $S^X = -\int dx\, N(x; \mu_X, s_X^2) \ln N(x; \mu_X, s_X^2) = \ln(2\pi e s_X^2)/2$, which explicitly decreases as s_X decreases.]

However, as proven in our previous paper [33], the advection-diffusion equation (1) always satisfies the H theorem, ensuring that the second law of thermodynamics remains valid in this process. This proof can be refined by exploiting the fact that the Wigner distribution function is bounded above and below [45],

$$|f^W(X, P, t)| \leqslant \frac{1}{\pi\hbar}, \tag{27}$$

so that the additional assumption of boundedness from below imposed in our previous work [33] is no longer required.

In the next section, we will analyze the entropy balance of this situation to show the entropy decrease concerning the uncertainty in the position of the particle does not contradict the second law of thermodynamics.

In the latter part of this section, we analyze the spatial distribution contraction in terms of $D^{(x)}(t)$ to provide a detailed explanation for the mechanism. The analytical solution of $D^{(x)}(t)$ for a general initial state was derived in our previous work [33] and is given by

$$D^{(x)}(t \geqslant \tau_{\rm rel}) = \bar{D} + \langle (X - \langle X\rangle_{t=0})(\sigma(P) - \langle \sigma(P)\rangle_{t=0})\rangle_{t=0} + t\langle (\sigma(P) - \bar{\sigma})^2\rangle_{\rm eq}, \tag{28}$$

where $\langle\cdot\rangle_{\rm eq} := \langle\cdot\rangle_{t\geqslant\tau_{\rm rel}}$ is the average over the local equilibrium Wigner distribution $f^W(X, P, t \geqslant \tau_{\rm rel})$, and

$$\bar{D} := \langle D(P)\rangle_{\rm eq} \quad \text{and} \quad \bar{\sigma} := \langle \sigma(P)\rangle_{\rm eq} \tag{29}$$

are the averaged transport coefficients. An alternative derivation of Eq. (28) has also been developed and is currently in preparation for publication.

A notable feature of this system is that, in addition to the first term of Eq. (28) representing diffusion, a second term that depends on the initial conditions and a third term that is linear in time also appear. These additional terms arise from the momentum dependence of the sound velocity $\sigma(P)$, and, therefore, represent the reversible phase-mixing effects [29].

Among these, the second term is the only term that can take negative values, as the first term is an average of the diffusion coefficient $D(P)$, which is always positive, and the third term is an average of a squared quantity.

The negativity of the second term depends on the initial conditions. This dependence arises because momentum relaxation occurs independently within each subspace $\mathcal{S}_{P_0}$, meaning that the equilibrium average retains a memory of the initial distribution.

A. Initial conditions for spatial contraction: Nonfactorizable Gaussian state

In our previous work [33], we considered a superposition of two Gaussian wave packets, which leads to Wigner distribution functions that exhibit negative regions due to quantum interference. In such cases, the functional $-\int f^W \ln f^W$ cannot be interpreted as entropy, making it unsuitable for analyzing entropy balance.

To overcome this limitation, here we employ a single Gaussian wave packet as the initial pure state. Gaussian pure states belong to a class of quantum states whose Wigner distribution functions are strictly nonnegative [44]. Moreover, in our system, the Wigner distribution function remains nonnegative at local equilibrium for such an initial state, and no negative regions appear thereafter.

Thus, starting from a Gaussian pure state eliminates the possibility that the spatial contraction could stem from "negative probability" regions in the Wigner distribution. Hence, we can rule out quantum interference artifacts as the origin of the spatial contraction.

Under this condition, the Wigner distribution function can be regarded as a joint probability distribution over coordinate and momentum variables [44]. Consequently, the functional $-\int dX dP\ f^W \ln f^W$ coincides with the standard nonequilibrium entropy, allowing us to analyze the entropy balance in a classical probabilistic sense, as discussed in Sec. IV.

Note that although we choose a pure initial state for the particle, the phonon bath is assumed to be in thermal equilibrium, and hence the total system is in a mixed state from the outset. Importantly, the mechanism of spatial contraction does not require the initial state for the particle to be pure. In practical implementations, mixed states could also lead to spatial contraction.

To induce spatial contraction, the initial state must be arranged so that different spatial regions exhibit opposite signs of the sound velocity $\sigma(P)$. Satisfying this requirement necessitates that different spatial regions must carry different momenta, meaning that there is a nonzero correlation between coordinates and momenta. Once such a correlation emerges, the distribution can no longer be factorized into independent functions of X and P.

For this purpose, we use a nonfactorizable Gaussian pure state whose Wigner distribution function is given as follows:

$$f^W(X, P, t = 0) = \frac{1}{\pi\hbar}\exp\left[-\frac{(P - P')^2}{2(\Delta P)^2} - \frac{(X - X' - \alpha P)^2}{2(\widetilde{\Delta X})^2}\right], \tag{30}$$

where the parameter ΔP represents the standard deviation of P and $\widetilde{\Delta X}$ is defined by the relation

$$\widetilde{\Delta X}\cdot\Delta P = \frac{\hbar}{2}. \tag{31}$$

The standard deviation ΔX of X is given by

$$\Delta X = \sqrt{(\widetilde{\Delta X})^2 + \alpha^2(\Delta P)^2}, \tag{32}$$

and therefore the state is not a minimum uncertainty state unless $\alpha = 0$. The parameters X' and P' represent the peak positions of the wave packet. The parameter α has the dimension X/P and introduces a momentum-dependent shift in the spatial distribution.

We can verify that the state (30) is a pure state under the condition (31). By applying a Fourier transformation to Eq. (30), we obtain the corresponding reduced density matrix:

$$f_k(P, t = 0) = \frac{1}{\sqrt{2\pi(\Delta P)^2}}\exp\left[-\frac{(P - P')^2}{2(\Delta P)^2} - \frac{(\widetilde{\Delta X})^2}{2}k^2 - i(X' + \alpha P)k\right], \tag{33}$$

which can be factorized with the condition (31) into the following form:

$$f_k(P, t = 0) = \psi_0\left(P + \frac{\hbar k}{2}\right)\psi_0^*\left(P - \frac{\hbar k}{2}\right), \tag{34}$$

where the wavefunction ψ_0 is written as

$$\psi_0(P) := (P|\psi_0) = \left[\frac{1}{2\pi(\Delta P)^2}\right]^{\frac{1}{4}} \exp\left[-\frac{(P-P')^2}{4(\Delta P)^2} - i\frac{P}{\hbar}X' - \frac{i}{\hbar}\frac{\alpha}{2}P^2\right]. \tag{35}$$

Here, the round bracket in the expression is normalized by the delta function as noted in Sec. II.

In the following, we describe the correlation between X and P in the initial distribution (30), which plays the essential role for spatial contraction. The presence of the $-\alpha P$ term in the exponent in Eq. (30) prevents the distribution from being factored into separate functions of X and P, which establishes the *nonzero correlation* between X and P. This correlation can be quantified by the correlation coefficient

$$r(t) := \frac{\mathrm{Cov}(X,P;t)}{\sqrt{\mathrm{Var}(X;t)\mathrm{Var}(P;t)}}, \tag{36}$$

where $\mathrm{Var}(X;t)$ and $\mathrm{Var}(P;t)$ are the variance of X and P, respectively, and $\mathrm{Cov}(X,P;t)$ is the covariance between X and P:

$$\mathrm{Var}(X;t) := \langle X^2\rangle_t - \langle X\rangle_t^2, \tag{37}$$

$$\mathrm{Var}(P;t) := \langle P^2\rangle_t - \langle P\rangle_t^2, \tag{38}$$

$$\mathrm{Cov}(X,P;t) := \langle (X-\langle X\rangle_t)(P-\langle P\rangle_t)\rangle_t. \tag{39}$$

Here, $\langle\cdot\rangle_t$ denotes averages over the Wigner distribution at time t. For the initial state (30), the correlation coefficient is $r(0) = \alpha\Delta P/\Delta X$, with $\mathrm{Var}(X;0) = (\Delta X)^2$, $\mathrm{Var}(P;0) = (\Delta P)^2$, and $\mathrm{Cov}(X,P;0) = \alpha(\Delta P)^2$. Hence, the sign of the initial correlation coefficient $r(0)$ is determined by the parameter α.

Next, we demonstrate that spatial contraction arises when this nonfactorizable Gaussian pure state is given as an initial state. However, the following argument does not necessarily have to satisfy Eq. (31), so it is valid even in mixed states. The Wigner distribution function under local equilibrium for the given initial state can be obtained by substituting Eq. (33) into Eqs. (19) and (20), yielding

$$f^W(X,P_\nu,t\gtrsim\tau_{\mathrm{rel}}) = \varphi^{\mathrm{eq}}_{P_0}(P_\nu)\sum_{\mu=-\infty}^{\infty}\frac{1}{\sqrt{2\pi(\Delta P)^2}}\frac{1}{\sqrt{2\pi\{(\widetilde{\Delta X})^2+2D(P_0)t\}}} \times\exp\left[-\frac{(P_\mu-P')^2}{2(\Delta P)^2} - \frac{(X-X'-\alpha P_\mu-\sigma(P_0)t)^2}{2\{(\widetilde{\Delta X})^2+2D(P_0)t\}}\right]. \tag{40}$$

Here, the summation over μ runs over all discrete momenta P_μ within the subspace $\mathcal{S}_{P_0}$ to which the discrete momentum P_ν belongs. Note that this function remains strictly nonnegative and that no negative regions appear at any $t \gtrsim \tau_{\mathrm{rel}}$.

By substituting $t = 0$ into Eq. (40), we can see the form of the initial distribution given in Eq. (30), indicating that the correlation between coordinate and momentum present in the initial state remains after the system reaches local equilibrium. In systems with two or more dimensions, relaxation occurs across the entire momentum space, and this summation over μ is replaced by an integral over the entire momentum space. As a result, the correlation between coordinate and momentum in the initial state vanishes at local equilibrium, and the distribution takes a form that is completely separable in the variables of coordinate X and momentum P. Hence, the persistence of correlation is a distinctive feature of the 1D system.

The time evolution of the Wigner distribution function (40) is depicted in Fig. 1. Here, we set the initial shift parameter α to be negative, and set the peak of the Gaussian at the origin $(X',P') = (0,0)$. At the initial state $t = 0$, the distribution exhibits a negative correlation between coordinate X and momentum P, as shown by the tilt of the elliptical contour in the X-P plane.

After reaching local equilibrium at $t = \tau_{\mathrm{rel}}$, the distribution splits into a central peak at $P_0 = P'$ and side peaks at $P_{\pm1}$ along the momentum axis. This splitting occurs because momentum transitions are restricted to the subspaces associated with the initial momentum distribution.

As shown in Fig. 1(b), while the main peak at P_0 exhibits a negative correlation, the side peaks at $P_{\pm1}$ (which also belong to the same subspace) show a positive correlation. This inversion of correlation occurs because the sign of the P_0 dependence of P_μ flips with μ:

$$\frac{dP_\mu}{dP_0} = (-1)^\mu. \tag{41}$$

Importantly, despite the flip in X-P_μ correlation, all peaks at P_μ share the same X-P_0 correlation (negative in the present case) originating from the initial state. Note that a necessary condition for spatial contraction is that the distribution exhibits a negative X-P_0 correlation.

As is evident from the contour plots, the wave packet is contracting in the spatial direction from $t = \tau_{\mathrm{rel}}$ to $t = \tau_{\mathrm{rel}} + 15$. This occurs because the sound velocity $\sigma(P)$ has opposite signs at opposite sign momenta P and $-P$, as shown in Eq. (25). Consequently, the distortion in the distribution, which reflects the negative correlation, gradually disappears.

At a later time, $t = \tau_{\mathrm{rel}} + 30$, the distortion reflecting the negative correlation almost disappears, and by $t = \tau_{\mathrm{rel}} + 40$, the distribution is instead distorted to exhibit positive correlation. In other words, the advection acts to contract the wave packet only until the negative correlation created in the initial state disappears. Beyond this time domain, the advection begins to work in the opposite direction, spreading the wave packet. It should also be noted that at all times, the diffusion effect works to spread the wave packet, gradually lowering its amplitude.

B. Analysis of the phenomenological diffusion coefficient

Next, we analyze the phenomenological diffusion coefficient $D^{(x)}(t)$ in the situation where apparent negative diffusion is occurring.

First, let us consider the diffusion term represented by the first term in the analytical solution (28):

$$\bar{D} := \langle D(P)\rangle_{t=\tau_{\mathrm{rel}}} = \int_{-\infty}^{\infty}dX\int_{-\infty}^{\infty}dP\, D(P) f^W(X,P,t=\tau_{\mathrm{rel}}) > 0. \tag{42}$$

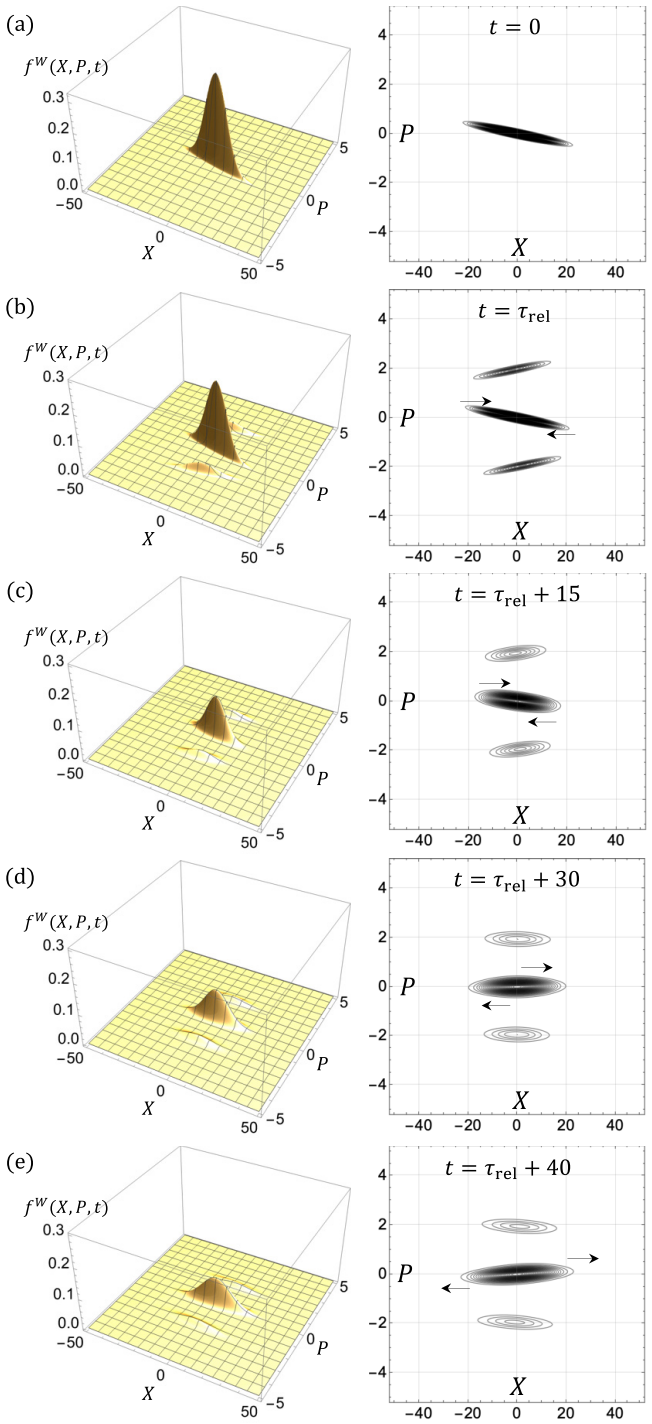

FIG. 1. Apparent negative diffusion with a single nonfactorizable Gaussian wave packet under the parameters chosen as $D^*/D_{\rm u} = 1$. All values are depicted in the units as defined in Eq. (A1). The left side shows bird's-eye views of the Wigner distribution function, and the right side presents contour plots. The arrows in the contour plots indicate the direction of momentum-dependent advection. The temperature is set to $T = 1$ in the aforementioned units. (a) Initial distribution at $t = 0$ with the negative shift parameter $\alpha = -40$ (in units of $x_{\rm u}/p_{\rm u}$). The peak of the Gaussian is set at the origin $(X', P') = (0, 0)$ with its width $\widetilde{\Delta X} = 3$. (b) Wigner distribution immediately after reaching local equilibrium at $t = \tau_{\rm rel}$. Since the initial momentum peak is set at $P_0 = P' = 0$, side peaks appear at $P_1(P_0) = 2$ and $P_{-1}(P_0) = -2$. (c) Wigner distribution at $t = \tau_{\rm rel} + 15$. Although diffusion spreads the wave packet, advection dominates, leading to the contraction of the wave packet in the spatial direction. (d) Wigner distribution at $t = \tau_{\rm rel} + 30$. The tilt in the contour of the distribution has almost vanished due to advection. (e) Wigner distribution at $t = \tau_{\rm rel} + 40$. At this stage, both the diffusion and the advection contribute to the spreading of the wave packet.

The reason this inequality holds is that the microscopic diffusion coefficient is always positive, $D(P) > 0$, and the Wigner distribution function integrated over X represents the true probability distribution for momentum:

$$\varphi(P,t) := \int_{-\infty}^{\infty} dX\, f^W(X,P,t) \geqslant 0. \tag{43}$$

Therefore, for any initial condition, the diffusion always contributes to the spreading of the wave packet.

Next, we focus on the second term, which depends on the initial distribution:

$$\begin{aligned}&\langle (X - \langle X\rangle_{t=0})(\sigma(P) - \langle\sigma(P)\rangle_{t=0})\rangle_{t=0} \\ &\quad = \langle X\sigma(P)\rangle_{t=0} - \langle X\rangle_{t=0}\langle\sigma(P)\rangle_{t=0}.\end{aligned} \tag{44}$$

This term arises due to the momentum dependence of the sound velocity $\sigma(P)$. Therefore, it represents a reversible phase-mixing effect. This term vanishes if the initial Wigner distribution function is factorizable into independent functions of X and P as

$$f^W(X,P,t=0) = \chi(X)\varphi(P). \tag{45}$$

The term (44) can also take either positive or negative values since the sound velocity $\sigma(P)$ can take both positive and negative values. When this term becomes negative, the reversible phase-mixing effect contributes to the contraction of spatial distribution, competing with the irreversible diffusion effect that spreads the distribution. Especially, if the condition

$$\bar{D} + \langle (X - \langle X\rangle_{t=0})(\sigma(P) - \langle\sigma(P)\rangle_{t=0})\rangle_{t=0} < 0 \tag{46}$$

holds, then apparent negative diffusion occurs. However, since this negative contribution of the phase mixing is a reversible effect, it does not contribute to the decrease of entropy.

Finally, let us focus on the third term in Eq. (28), which depends linearly on time t. This term also arises because the sound velocity $\sigma(P)$ depends on momentum, reflecting the effect of phase mixing. However, unlike the second term, this term always contributes to the spreading of the wave packet, because the condition

$$t\langle(\sigma(P) - \bar{\sigma})^2\rangle_{\rm eq} > 0 \tag{47}$$

holds. Furthermore, the third term increases linearly with time, leading to anomalous diffusion. The anomalous diffusion caused by this phase-mixing effect is discussed in detail in Ref. [29].

Figure 2 shows the time evolution of the phenomenological diffusion coefficient $D^{(x)}(t)$ as the solid line, corresponding to the situation depicted in Fig. 1. Initially, $D^{(x)}(t)$ takes negative values. This indicates that the reversible phase-mixing effect, which provides the negative contribution, overwhelms the positive contribution from diffusion, leading to the contraction of the wave packet in the spatial direction at that time.

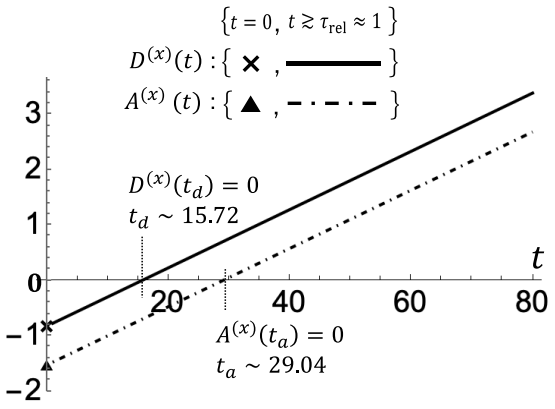

FIG. 2. Time evolution of the phenomenological diffusion coefficient $D^{(x)}(t)$ and the effect excluding the diffusion effect $A^{(x)}(t) = D^{(x)}(t) - \bar{D}$ in the situation depicted in Fig. 1. The relaxation time (in units of $t_{\rm u}$) is $\tau_{\rm rel} \approx 1$ under the parameters chosen as $D^* = D_{\rm u}$. The cross marks represent $D^{(x)}(0)$, the solid line shows $D^{(x)}(t \gtrsim \tau_{\rm rel})$, the triangle marks indicate $A^{(x)}(0)$, and the dash-dotted line depicts $A^{(x)}(t \gtrsim \tau_{\rm rel})$. The time t_d satisfies $D^{(x)}(t_d) = 0$, which corresponds to the threshold time, at which contraction turns into expansion, resulting in the minimum width of the spatial distribution. Additionally, the time t_a satisfies $A^{(x)}(t_a) = 0$, at which the negative tilt in the contour of the distribution turns into a positive one.

However, due to the positive phase-mixing effect (47), which provides the positive time-linear contribution, $D^{(x)}(t)$ turns to be positive and the wave packet begins to expand.

The threshold time t_d, at which $D^{(x)}(t_d) = 0$ satisfies and contraction turns into expansion, is given by

$$t_d = \frac{-\langle (X - \langle X\rangle_{t=0})(\sigma(P) - \langle \sigma(P)\rangle_{t=0})\rangle_{t=0} - \bar{D}}{\langle (\sigma(P) - \bar{\sigma})^2\rangle_{\rm eq}}. \tag{48}$$

In Fig. 2, $t_d \sim 15.72$ with the time unit $t_{\rm u} = \hbar/mc^2$, which approximately corresponds to the situation at $t = \tau_{\rm rel} + 15$ in Fig. 1. One can see that at $t = \tau_{\rm rel} + 15$ in Fig. 2, the tilt in the contour of the distribution has not yet disappeared. Nevertheless, the phenomenological diffusion coefficient $D^{(x)}(t)$ turns to positive, indicating the beginning of wave packet expansion.

To understand this behavior, we decompose $D^{(x)}(t)$ into its reversible and irreversible contributions by subtracting the irreversible diffusion term $\bar{D}$, leading to the definition

$$A^{(x)}(t) := D^{(x)}(t) - \bar{D}. \tag{49}$$

This represents the diffusion-free component that arises solely from reversible phase-mixing effects.

The time evolution of $A^{(x)}(t)$ is plotted as the dash-dotted line in Fig. 2. The threshold time t_a, at which $A^{(x)}(t_a) = 0$, is greater than t_d and is given by

$$t_a = -\frac{\langle (X - \langle X\rangle_{t=0})(\sigma(P) - \langle \sigma(P)\rangle_{t=0})\rangle_{t=0}}{\langle (\sigma(P) - \bar{\sigma})^2\rangle_{\rm eq}}. \tag{50}$$

In Fig. 2, $t_a \sim 29.04$, which approximately corresponds to the situation at $t = \tau_{\rm rel} + 30$ in Fig. 1. At this point, the tilt in the contour of the distribution has nearly disappeared due to advection. For $t > t_a$, the tilt gradually reappears in the opposite direction as advection continues.

In summary, the initial conditions create a competition between reversible advection, which contracts the distribution, and irreversible diffusion, which always expands the distribution. When advection is sufficiently strong compared to diffusion, the spatial distribution contracts. The contribution of advection changes over time. Initially, advection counteracts diffusion, leading to the spatial contraction. However, beyond a finite time t_a (which depends on the initial shift parameter α), the advection effect starts to contribute to the expansion of the distribution. The minimum width of the spatial distribution is reached at a time $t_d < t_a$, due to the interplay between advection and diffusion.

Since the diffusion effect depends on temperature, it is natural to examine how increasing temperature modifies this balance. As the diffusion effect represented by $\bar{D}$ strengthens with increasing temperature, it gradually reduces the time t_d and the time interval

$$\tau_{\rm rel} \lesssim t \leqslant t_d, \tag{51}$$

where the spatial contraction can be observed, diminishes. Above a threshold temperature, the difusion dominates and the system does not exhibit the spatial contraction. In Fig. 11 in Appendix D, we show this threshold temperature, using parameter values relevant to the protein molecular chain.

IV. ENTROPY BALANCE DURING THE SPATIAL DISTRIBUTION CONTRACTION

The previous section illustrates a situation where the spatial distribution of a Brownian particle in one-dimensional quantum system contracts without releasing heat to the environment, and the H theorem still holds. However, what compensates for the decrease in entropy associated with this contraction of the spatial distribution? In this section, we answer this question by analyzing the entropy balance in the situation.

First, we discuss the method of defining entropy using the Wigner distribution function. In general, the Wigner distribution function is a quasijoint probability distribution over coordinate and momentum, which, due to the uncertainty principle, can take negative values. Therefore, if one defines nonequilibrium entropy in the form of $-\int dX dP\ f^W \ln f^W$, the entropy value may have an imaginary part, and it is problematic.

However, in the situation of Sec. III, where the initial state is given as a single Gaussian wave packet, the Wigner distribution function remains non-negative throughout its time evolution, and it becomes a joint probability distribution over coordinate and momentum variables [44]. Therefore, in this specific case, we can define entropy using the Wigner distribution function as follows:

$$S(t) := -\int dX \int dP\ f^W(X, P, t) \ln \left\{ f^W(X, P, t) \Big/ \frac{1}{\pi\hbar} \right\}. \tag{52}$$

Here, the factor $1/\pi\hbar$ inside the logarithm is to make the expression dimensionless. Since the Wigner distribution function has upper and lower bounds [see Eq. (27)], the factor $1/\pi\hbar$ guarantees that the entropy $S(t)$ takes positive values.

Since $f^W(X,P,t) \geqslant 0$ in this case, the entropy $S(t)$ increases monotonically, in agreement with the proof of the H theorem [33].

This entropy can be identically decomposed as follows:

$$S(t) = S^X(t) + S^P(t) - S_I^{X:P}(t), \tag{53}$$

where

$$S^X(t) := -\int dX\ \chi(X,t) \ln\left\{\chi(X,t)\Big/\frac{1}{\Delta_\chi}\right\}, \tag{54}$$

$$S^P(t) := -\int dP\ \varphi(P,t) \ln\left\{\varphi(P,t)\Big/\frac{1}{\Delta_\varphi}\right\}, \tag{55}$$

$$S_I^{X:P}(t) := \int dX \int dP\ f^W(X,P,t) \ln\left\{\frac{f^W(X,P,t)}{\chi(X,t)\varphi(P,t)}\right\}, \tag{56}$$

and $\chi(X,t)$ and $\varphi(P,t)$ are the marginal probability distributions for coordinate and momentum, respectively:

$$\chi(X,t) = \int dP\ f^W(X,P,t), \tag{57}$$

$$\varphi(P,t) = \int dX\ f^W(X,P,t). \tag{58}$$

The factors Δ_χ and Δ_φ inside the logarithms in Eqs. (54) and (55) are used to make the expressions dimensionless, and they satisfy

$$\Delta_\chi \cdot \Delta_\varphi = \pi\hbar. \tag{59}$$

Here, we choose

$$\Delta_\chi = \sqrt{2\pi(\widetilde{\Delta X})^2}, \quad \Delta_\varphi = \sqrt{2\pi(\Delta P)^2}. \tag{60}$$

Since these factors, Δ_χ and Δ_φ, do not contribute to the time evolution of each entropy term, they are not essential for the subsequent discussion.

The entropy of the spatial distribution, $S^X(t)$, represents the uncertainty in the coordinate of the particle, while the entropy of the momentum distribution, $S^P(t)$, represents the uncertainty in the particle's momentum. Additionally, $S_I^{X:P}(t)$ represents the mutual information between coordinate and momentum [46]. This quantity is defined as the relative entropy (Kullback-Leibler divergence) [37] between the joint probability distribution $f^W(X,P,t)$ and the product of the marginal distributions $\chi(X,t)\varphi(P,t)$. The mutual information $S_I^{X:P}(t)$ quantifies the degree of correlation between X and P. It can be proven that $S_I^{X:P}(t)$ is always non-negative [46], and a decrease in $S_I^{X:P}(t)$ contributes to an increase in the overall entropy $S(t)$.

The identity (53) suggests that the spatial distribution entropy $S^X(t)$ may decrease, yet the total entropy $S(t)$ continues to increase, because this decrease is exactly compensated by a reduction in the mutual information $S_I^{X:P}(t)$.

However, in classical Brownian motion, it is assumed that the momentum distribution relaxes to the Maxwellian distribution, independent of the spatial distribution. As a result, the mutual information decreases to $S_I^{X:P}(t) = 0$, leaving no room for a decrease at local equilibrium, and thus the above entropy balance is not possible.

On the other hand, in the one-dimensional quantum Brownian motion, the mutual information remains greater than zero even after reaching local equilibrium since the joint probability distribution at local equilibrium is nonseparable between X and P, as given in Eqs. (19) and (20):

$$S_I^{X:P}(t \gtrsim \tau_{\rm rel}) = \int dX \int_{-mc}^{mc} dP_0 \sum_{\nu=-\infty}^{\infty} \chi_{P_0}(X,t)\varphi_{P_0}^{\rm eq}(P_\nu) \times \ln\left\{\frac{\chi_{P_0}(X,t)\varphi_{P_0}^{\rm eq}(P_\nu)}{\chi(X,t)\varphi(P_\nu,t)}\right\} > 0. \tag{61}$$

Here, the relations between $\chi(X,t)$ and $\chi_{P_0}(X,t)$, and between $\varphi(P_\nu,t)$ and $\varphi_{P_0}^{\rm eq}(P_\nu)$ are as follows [with use of relation (24)]:

$$\chi(X, t \gtrsim \tau_{\rm rel}) = \int_{-mc}^{mc} dP_0 \sum_{\nu=-\infty}^{\infty} \chi_{P_0}(X,t)\varphi_{P_0}^{\rm eq}(P_\nu) = \int_{-mc}^{mc} dP_0\ \chi_{P_0}(X,t), \tag{62}$$

$$\varphi(P_\nu, t \gtrsim \tau_{\rm rel}) = \int dX\ \chi_{P_0}(X,t)\varphi_{P_0}^{\rm eq}(P_\nu) = \varphi^{\rm init}(P_0)\varphi_{P_0}^{\rm eq}(P_\nu). \tag{63}$$

Here, we define the conserved weight in each subspace by

$$\begin{aligned}\varphi^{\rm init}(P_0) &:= \int dX\ \chi_{P_0}(X,t) \\ &= \int dX\ \frac{1}{2\pi}\int dk\ e^{ikX} e^{-\{ik\sigma(P_0)+k^2D(P_0)\}t} \sum_\mu f_k(P_\mu(P_0),0) \\ &\overset{(a)}{=} \int dk\ \delta(k)\ e^{-\{ik\sigma(P_0)+k^2D(P_0)\}t} \sum_\mu f_k(P_\mu(P_0),0) \\ &= \sum_\mu f_0(P_\mu(P_0),0) = \sum_\mu \varphi(P_\mu(P_0),0),\end{aligned} \tag{64}$$

where (a) uses $\int dX\ e^{ikX} = 2\pi\delta(k)$ under the Fourier convention in Eq. (7). Hence, $\varphi^{\rm init}(P_0)$ is a conserved quantity within each $\mathcal{S}_{P_0}$, determined by initial momentum distribution.

The time derivatives of the entropies (54), (55), and (56) are written as follows:

$$\frac{d}{dt}S^X(t) = -\frac{d}{dt}\int dX\ \chi(X,t)\ln\chi(X,t), \tag{65}$$

$$\frac{d}{dt}S^P(t) = 0, \tag{66}$$

$$\frac{d}{dt}S_I^{X:P}(t) = -\frac{d}{dt}\int dX\ \chi(X,t)\ln\chi(X,t) + \frac{d}{dt}\int_{-mc}^{mc} dP_0 \int_{-\infty}^{\infty} dX\ \chi_{P_0}(X,t)\ln\chi_{P_0}(X,t). \tag{67}$$

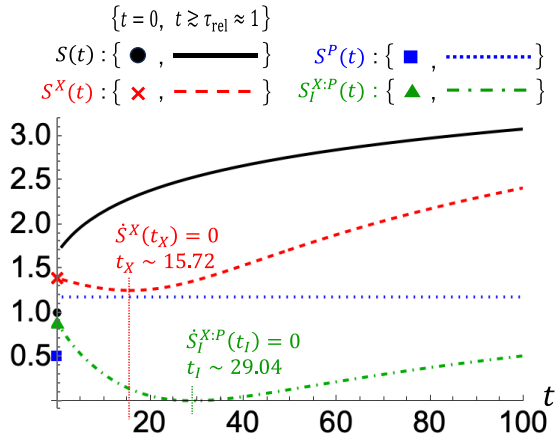

FIG. 3. The time evolution of entropies in the situation discussed in Fig. 1 is shown at the initial time $t = 0$ and in the region $t \gtrsim \tau_{\rm rel}$. The black circle represents $S(0)$, the solid line represents $S(t \gtrsim \tau_{\rm rel})$, the red cross represents $S^X(0)$, the dashed line represents $S^X(t \gtrsim \tau_{\rm rel})$, the blue square represents $S^P(0)$, the dotted line represents $S^P(t \gtrsim \tau_{\rm rel})$, and the green triangle represents $S_I^{X:P}(0)$, with the dot-dashed line representing $S_I^{X:P}(t \gtrsim \tau_{\rm rel})$. Note that although the black solid line and blue dotted line appear to show a discontinuous jump between $t = 0$ and $t = \tau_{\rm rel}$, these values are actually continuous. This apparent discontinuity arises because the momentum relaxation process occurs on a much shorter timescale than that of spatial relaxation. We do not plot the entropy evolution during this rapid relaxation period, as no analytical expression is available in this interval. The time at which the entropy of the spatial distribution $S^X(t)$ reaches its minimum is $t_X \sim 15.72$ (in units of $t_{\rm u}$), and the time at which the mutual information $S_I^{X:P}(t)$ reaches its minimum is $t_I \sim 29.04$. These times coincide with t_d and t_a in Fig. 2.

Thus, the time derivative of the total entropy $S(t)$ is as follows:

$$\begin{aligned}\frac{d}{dt}S(t) &= \frac{d}{dt}S^X(t) - \frac{d}{dt}S_I^{X:P}(t)\\ &= -\frac{d}{dt}\int_{-mc}^{mc} dP_0 \int_{-\infty}^{\infty} dX\ \chi_{P_0}(X,t)\ln\chi_{P_0}(X,t)\\ &= -\int_{-mc}^{mc} dP_0\, D(P_0)\int_{-\infty}^{\infty} dX\left[\frac{\{\frac{\partial}{\partial X}\chi_{P_0}(X,t)\}^2}{\chi_{P_0}(X,t)}\right] \geqslant 0.\end{aligned} \tag{68}$$

In going from the second to the third line, we use that $\chi_{P_0}(X,t)$ directly follows an advection-diffusion equation obtained from Eq. (1), and performs integration by parts over X. The final inequality holds because $\chi_{P_0}(X,t) \geqslant 0$ in the situation considered in Sec. III.

Whether the spatial distribution entropy $S^X(t)$ increases or decreases, it is completely compensated by the first term of the time derivative of $S_I^{X:P}(t)$ in Eq. (67), so it does not contribute to the change in the total entropy $S(t)$.

The entropy balance in the case discussed in Sec. III is shown in Fig. 3. Note that the figure depicts the values of each entropy term at the initial time $t = 0$, as well as their changes over time in the region $t \gtrsim \tau_{\rm rel}$. The spatial distribution entropy $S^X(t)$ decreases for a while and then begins to increase. This behavior is consistent with the behavior of the wave packet in Fig. 1, where the wave packet initially contracts and then starts expanding. At the same time, the mutual information $S_I^{X:P}(t)$ also decreases for a short time, before it begins to increase. As a result, the decrease in $S^X(t)$ is compensated, and the total entropy $S(t)$ continues to increase monotonically. Additionally, since the momentum distribution has relaxed to equilibrium at $t = \tau_{\rm rel}$, the momentum entropy $S^P(t)$ remains at its maximum value for $t \gtrsim \tau_{\rm rel}$ without further change.

In this entropy balance of the Brownian motion in the one-dimensional quantum system, the mutual information between the spatial distribution and momentum distribution formed in the initial state is maintained even in the local equilibrium state, and the mutual information reduces the entropy of the spatial distribution. This means the uncertainty regarding the particle's coordinate can be reduced by utilizing the correlation between coordinate and momentum. Once the initial correlation is established, this reduction in entropy of spatial distribution occurs naturally as the system evolves with a fixed Hamiltonian, requiring no external energy input, making the process highly efficient. This indicates that Brownian particles can be controlled in an energy-efficient manner with minimal heat generation, offering advantages in realizing a forward bias and the completion of the computation in Brownian computers.

This aligns with the framework of an information ratchet [47,48], where state changes are driven by information with minimal external energy supply. In an information ratchet, the entropy of a spatial distribution can be reduced through feedback control based on the system's internal information, without directly performing work on the system. This approach is rooted in the concept of Maxwell's demon, which uses information to perform thermodynamic operations. In classical Brownian motion systems and other typical thermodynamic systems, an overdamped regime is assumed, where the momentum distribution quickly relaxes to a Maxwell distribution and becomes statistically independent of the spatial distribution. As a result, it is impossible to create and utilize a correlation between coordinate and momentum. Therefore, Maxwell's demon requires an external degree of freedom, namely, the demon's memory, to create a correlation with the particle's coordinate X. The demon uses this correlation to control the particle's position. In this case, the reduction in system entropy is explained consistently with the second law of thermodynamics through a decrease in the mutual information between the system and the external memory [32].

On the other hand, in 1D quantum Brownian motion, the relaxation occurs within each subspace independently, so even after local equilibrium is established, the momentum distribution and spatial distribution remain nonseparable. In other words, X and P remain correlated. Therefore, the momentum P, which is the dynamical variable conjugate to coordinate X, can be used in place of an external memory. The advantage of using momentum is that it eliminates the need to introduce the abstract concept of feedback control by an external entity, such as Maxwell's demon. If an appropriate correlation between X and P is established in the initial state, the system dynamics will naturally reduce the entropy of the spatial distribution through a reversible phase-mixing effect caused by the momentum dependence of the sound velocity $\sigma(P)$.

V. CONCLUDING REMARKS

In this paper, we investigated Brownian motion in a 1D quantum system to examine whether it can serve as a physical foundation for Brownian computing. Our primary goal was to clarify the thermodynamic consistency of unidirectional transport that occurs without any external force and associated energy dissipation. We demonstrated that, in such a system, spatial distribution contraction arises naturally and remains fully consistent with the second law of thermodynamics. These results provide a thermodynamically consistent mechanism for directional Brownian motion and offer a theoretical basis for energy-efficient computation using 1D quantum Brownian motion.

The underlying mechanism of unidirectional transport and spatial distribution contraction lies in the partitioning of the particle's momentum space into subspaces that lack momentum inversion symmetry. Such partitioning leads to the preservation of an initial correlation between coordinate and momentum even after momentum relaxation. This remaining correlation, in turn, plays a crucial role in enabling entropy reduction in the spatial distribution. Notably, the reduction is driven by a reversible phase-mixing effect that arises from the momentum dependence of the transport velocity in each momentum subspace.

To induce spatial distribution contraction, we employed a single nonfactorizable Gaussian wave packet as the initial state. In this case, the corresponding Wigner distribution function contains no negative regions, allowing it to be regarded as a joint probability distribution in coordinate-momentum space. This makes it possible to define a conventional nonequilibrium entropy using the Wigner distribution function. Consequently, the relative entropy, which quantifies coordinate-momentum correlations as mutual information, naturally emerges in the analysis. This provides a consistent explanation for the decrease in spatial distribution entropy, without violating the second law of thermodynamics.

These phenomena arise as a consequence of quantum dissipation in the spatially constrained 1D system. In the classical limit $\hbar \to 0$, the collision operator vanishes, and dissipation no longer exists [see the explanation below Eq. (11)]. Hence, the dissipation in the 1D system is purely a quantum effect, and these phenomena inherently require both one-dimensionality and quantum nature.

Nevertheless, discussions of Brownian computing often rely on the hypothesized existence of classical 1D Brownian motion, based on phenomenological arguments. However, as our analysis shows, such motion is not microscopically justified in our model. Therefore, the comparisons made below between existing models of Brownian computers and our quantum model are conducted under the hypothesis that classical 1D Brownian motion exists.

Brownian computers, which harness thermal fluctuations near equilibrium, have been expected to achieve ultra-low-energy computation. However, directing classical Brownian motion incurs certain costs. Specifically, because the Maxwellian momentum distribution is inversion-symmetric, the particle does not possess a statistical "direction," making it necessary to induce drift not only to drive the computation forward but also to increase the reliability of completing computations.

In contrast, the Brownian motion in a 1D quantum system offers advantages in terms of manageability compared to its classical counterpart. The asymmetric Maxwellian distributions formed in each momentum subspace result in a nonzero transport velocity [i.e., sound velocity $\sigma(P)$]. The transport coefficients depend on the momentum. Moreover, because relaxation occurs separately in each subspace, coordinate-momentum correlations present in the initial state persist even after momentum relaxation. Through appropriate preparation of the initial state, it is thus possible to control the Brownian particle near thermal equilibrium without requiring extensive external intervention.

Let us consider a comparison with scenarios resembling Maxwell's demon—so-called "information ratchets" [47,48]—where classical Brownian particles are guided via external observation and feedback control. In such settings, an external memory is introduced to correlate the particle's coordinate with that memory, thereby controlling the Brownian particle. On the other hand, in our 1D quantum system, there exists an intrinsic correlation between the coordinate and its conjugate dynamical variable, momentum. As a result, the system's internal dynamics alone can effectively steer the Brownian particle without the need for an external feedback mechanism.

Importantly, the presence of partitioning in momentum space, which is a manifestation of the 1D quantum effect, is temperature independent. It is therefore possible that quantum effects remain even at relatively high temperatures, and the resulting one-way transport remains valid.

At the same time, we note that in the asymptotic high-temperature limit, the sound velocity $\sigma(P_0)$ gradually vanishes, and the particle's motion approaches classical behavior because positive and negative contributions from thermally excited momentum states cancel out. We further analyze the high-temperature condition in Appendix C, where it is related to the crossover in phonon statistics from quantum to classical [see Eq. (C12)]:

$$T \gg T_{\mathrm{u}}, \quad T_{\mathrm{u}} = mc^2/k_{\mathrm{B}}. \tag{69}$$

The characteristic scale T_{u} can, however, be rather high depending on the system parameters. For example, using the parameters of an α-helical protein molecular chain [34,40,49], the temperature can be estimated as $T_{\mathrm{u}} \sim 200$ K, where the effective mass is $m \simeq 2 \times 10^{-28}$ kg and the propagation speed of acoustic phonons is $c \simeq 4000$ m/s. In this unit, the room temperature $T = 300$ K corresponds to $T/T_{\mathrm{u}} = 1.5$, indicating that the unidirectional transport remains effective even at such temperatures (see Fig. 10). When estimated using semiconductor parameters [41], for example those of GaAs, the unit temperature becomes $T_{\mathrm{u}} \sim 0.09$ K, with $m \simeq 6 \times 10^{-32}$ kg and $c \simeq 5000$ m/s. This value is considerably lower than that of the protein system. The difference in temperature scale is primarily due to the difference in the effective mass m of the particle: In the α-helical protein, the particle is a vibrational exciton of a C=O molecule, whereas in semiconductors, the particle is an electron with a much smaller effective mass. However, our results also suggest that the temperature can be increased by using ions instead of electrons, even in the case of semiconductors.

As a related study, a technique called "momentum computing" has been proposed [17,50]. This approach aims to realize computation by switching between Brownian motion and dynamically reversible (harmonic) motion, addressing the difficulties of Brownian computing arising from the lack of a statistical "direction" in the Brownian motion. Doing so requires temporarily decoupling the system from the thermal bath to create conditions under which the particle can move reversibly by its momentum. In contrast, in the 1D quantum Brownian motion described here, the system remains continuously coupled to the thermal bath, and unidirectional transport is achieved simply by setting the initial momentum state. Without needing to disconnect from the thermal bath, the interplay of quantum dissipative effects and the choice of initial conditions allows one to steer the Brownian particle's motion.

Finally, while the present study has focused on the fundamental physics of 1D quantum Brownian motion, we also outline in Appendix B how the pseudoratchet effect may be applied in Brownian computing. This provides a conceptual link between the microscopic mechanism studied here and possible circuit-level implementations.

In this study, we have not discussed the cost associated with preparing the initial states necessary to achieve unidirectional transport or spatial distribution contraction. Evaluating such costs and considering the applicability of these conditions in experimental settings remain important challenges for future research. Nonetheless, as shown in this paper, the finding that quantum dissipation in the 1D system can spontaneously give rise to unidirectional transport without contradicting the second law of thermodynamics provides an avenue for ultra-low-energy computation and will strongly motivate further developments in this field.

ACKNOWLEDGMENTS

We thank Hiroaki Umehara for pointing out the potential of using the transport properties of 1D quantum Brownian motion for ratchet applications, which motivated us to pursue the analysis further. This work was supported by JST CREST Grant No. JPMJCR20C1 and JSPS KAKENHI Grant No. JP24K00547.

DATA AVAILABILITY

No data were created or analyzed in this study.

APPENDIX A: UNIDIRECTIONAL TRANSPORT AS PSEUDORATCHET

In this Appendix, we illustrate the unidirectional transport of a 1D quantum Brownian particle, initially prepared as a minimum-uncertainty wave packet.

A similar situation was already presented in our previous work [29], but here we highlight a key feature that was not emphasized before: The direction of transport in local equilibrium is not determined by the sign of the initial momentum itself, but rather by the momentum subspace to which the initial momentum belongs. As a result, the transport can even occur in the direction opposite to the initial momentum, as shown in Fig. 4.

This confirms that the directed motion is not simply a persistence of the initial inertia (as in underdamped motion), but instead a structure emerging in local equilibrium, which is therefore robust against noise.

The figure is presented in dimensionless units. The units for coordinate, momentum, time, and temperature are, respectively, given by

$$x_{\mathrm{u}} = \frac{\hbar}{mc}, \quad p_{\mathrm{u}} = mc, \quad t_{\mathrm{u}} = \frac{\hbar}{mc^2}, \quad T_{\mathrm{u}} = \frac{mc^2}{k_{\mathrm{B}}}, \tag{A1}$$

where k_{B} is the Boltzmann constant. This choice of units corresponds to setting $m = 1$, $c = 1$, $\hbar = 1$, and $k_{\mathrm{B}} = 1$. Throughout this paper, all figures are presented using these units.

We define the characteristic scale of the diffusion coefficient as

$$D^* = \frac{\hbar^2 \rho_M c^3}{m\Delta_0^2}, \tag{A2}$$

which is determined from the microscopic kinetic analysis of this model [29]. To simplify the numerical analysis and highlight the intrinsic dynamics of the system, we choose the parameters ρ_M and Δ_0 such that D^* becomes equal to the unit of diffusion $D_{\mathrm{u}} = x_{\mathrm{u}}^2/t_{\mathrm{u}} = \hbar/m$, i.e., $D^*/D_{\mathrm{u}} = 1$.

This pseudoratchet behavior provides the physical basis for energy-efficient directional control of Brownian particles, which can be directly exploited in Brownian circuits, as discussed in Appendix B.

APPENDIX B: ROLE OF THE PSEUDORATCHET IN BROWNIAN COMPUTING

This Appendix shows how the pseudoratchet effect of 1D quantum Brownian motion can be exploited in Brownian computing. To this end, we describe Brownian circuits [8–10], a computational architecture that uses Brownian particles as signal carriers (*tokens*).

In a Brownian circuit, each token moves randomly along wires and interacts locally at gate elements. This architecture leverages the stochastic exploration of the signal path for robust and clock-free computation with simple gate elements.

The architecture is built from two types of gate elements, shown in Fig. 5:

(1) Hub: This element functions as a symmetric three-way junction, allowing tokens to freely roam among the three connected wires with equal probability.

(2) Conservative join (CJoin): This element has two input wires and two output wires. When one token is present on each input wire simultaneously, both are absorbed and two tokens are emitted on the output wires. If only one arrives, it remains pending until the other arrives, or until the pending token backtracks out of its pending position via Brownian motion.

This set of elements has been proven to be primitives for Brownian circuits [8], forming a computationally universal set.

As an example, Fig. 6 shows a Brownian circuit with the functionality of a Half-Adder (see Table I) that is solely

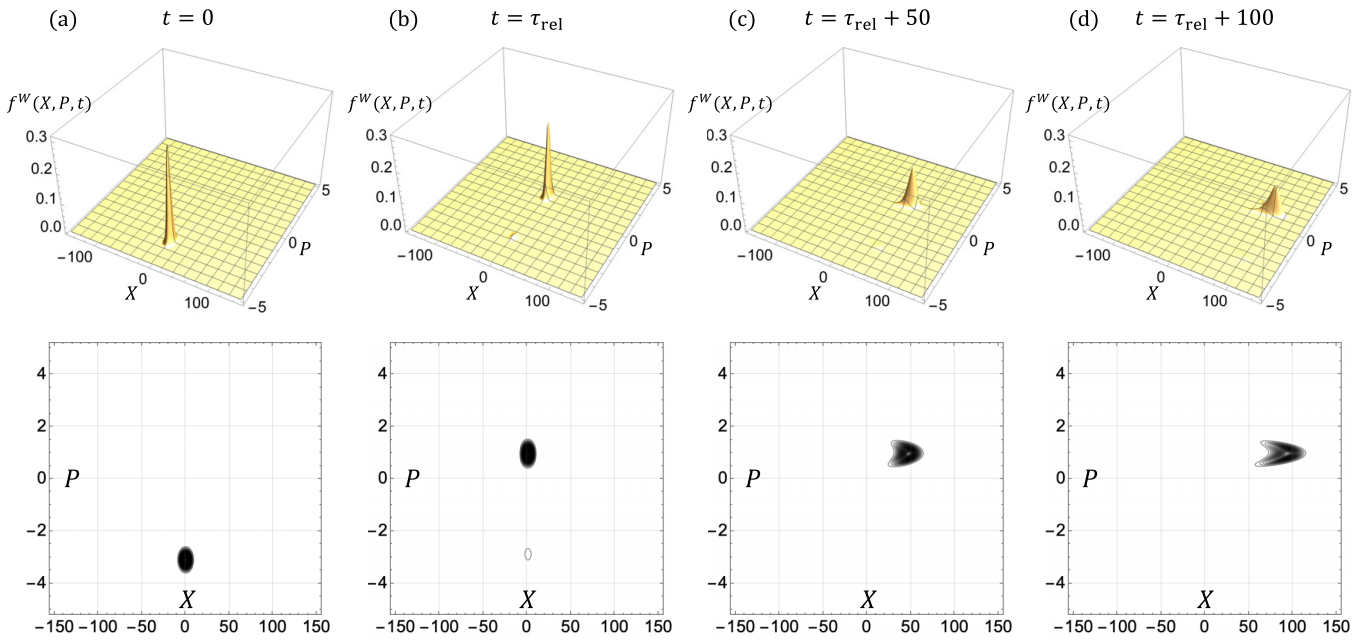

FIG. 4. Unidirectional transport of a one-dimensional quantum Brownian particle under the parameters chosen as $D^*/D_{\rm u} = 1$. All values are depicted in the units defined in Eq. (A1). The temperature is set to $T = 1$. The time evolution of the wave packet in this setup was previously derived (see Eq. (88) in Ref. [29]). This is the case $\alpha = 0$ in Eq. (40). Unlike free particle propagation, even when a particle is initially given negative momentum, the particle propagation at local equilibrium $t \gtrsim \tau_{\rm rel}$ occurs in the positive spatial direction. Note that during the relaxation period ($t = 0$ to $t = \tau_{\rm rel}$), the momentum distribution of the particle relaxes to the thermal equilibrium in each subspace with the temperature of the phonons. (a) Initial Wigner distribution at $t = 0$ with a momentum peak at $P' = -3.1$ with width $\Delta X = 3$. This peak momentum belongs to the subspace $P_0 = 0.9$, which means $P' = P_2(0.9) = -3.1$. (b) Wigner distribution immediately after reaching local equilibrium at $t = \tau_{\rm rel}$. Since momentum transfer occurs only within the subspace to which the initial momentum belongs, the equilibrium momentum distribution has a peak at $P_0 = 0.9$ with a small side peak at $P_2(0.9) = -3.1$. As the temperature increases, additional side peaks emerge at discrete momenta $P_\nu(0.9)$. (c), (d) The Wigner distributions at $t = \tau_{\rm rel} + 50$ and $t = \tau_{\rm rel} + 100$, respectively. The distribution moves in the positive X direction with the sound velocity $\sigma(0.9) > 0$.

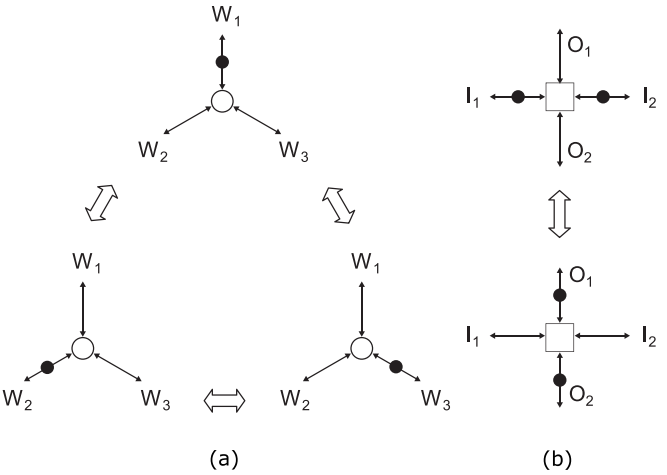

FIG. 5. Brownian circuit primitives that form a complete set from which any Brownian circuit can be constructed [8]. (a) Hub and its possible transitions. A token is denoted by a black blob. Fluctuations cause a token to move between any of the Hub's three wires W_1, W_2, and W_3 in any order. (b) CJoin and its possible transitions. If there is a token on only one input wire (I_1 or I_2), this token remains pending until a signal arrives on the other input wire. These two tokens will then result in one token on each of the two output wires O_1 and O_2. If there is only one pending token, it may backtrack through Brownian motion to another part of the circuit.

built from Hubs and CJoins. In this circuit, the inputs and outputs are *dual-rail encoded*, which means that each signal path consists of two wires—one wire labeled 0 and one wire labeled 1—that carry a binary signal through the presence of

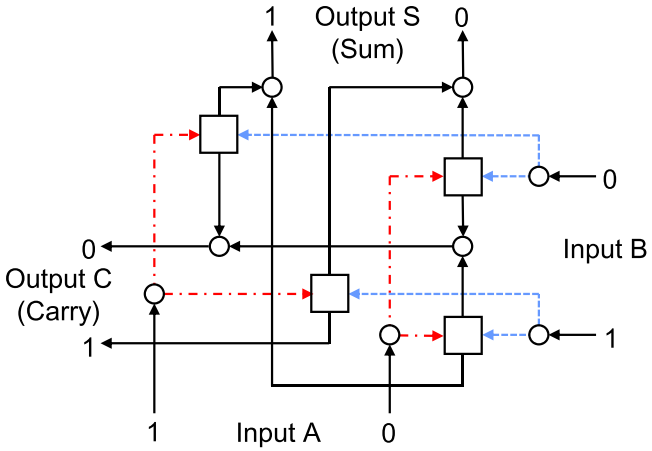

FIG. 6. Brownian circuit for a Half-Adder. Signal paths are dual-rail encoded. Binary signals on the two inputs result in the corresponding Sum and Carry outputs. The red (dot-dashed) wires, corresponding to input A, and the blue (dashed) wires, corresponding to input B, indicate the locations where random search is required for the circuit to work properly.

TABLE I. Truth table of the Half-Adder, with A and B representing binary inputs, and C and S denoting the corresponding outputs (Carry and Sum, respectively).

A	B	C	S
0	0	0	0
0	1	0	1
1	0	0	1
1	1	1	0

a token on one of the wires, and the absence of a token on the other wire, while the absence of tokens on both wires signifies a pause between subsequent signals. Under this definition, tokens occurring simultaneously on both wires are not allowed. The Half-Adder has two input signal paths, which represent the signals to be added, as well as two output paths, representing the sum and the carry.

The Half-Adder contains four CJoins, one for each combination of binary inputs, i.e., 00, 01, 10, and 11. Through a network of Hubs just after the input, the two input signals search their way to the CJoin corresponding to the binary input combination, going back and forth through Brownian motion, in the process visiting CJoins that have no matching second signals, but eventually settling for the CJoin that can accept both signals.

This random search is an essential part of Brownian circuits: Without it, they cannot operate deadlock-free, as shown in Ref. [9]. However, it comes at a cost in terms of computation time. After the input signals have been absorbed by the correct CJoin, the corresponding two output signals find their way through a network of Hubs to the corresponding sum and carry outputs, but on this path, no random search is necessary, because there is only one choice for the final destination. Brownian motion of the output signals, however, may make their journey to their destination quite time-consuming. In order to limit the time that signals engage in unnecessary random search, a third circuit primitive is introduced in Ref. [8], the *Ratchet* (Fig. 7).

Though not strictly necessary for a complete set of primitives from which any Brownian circuit can be constructed, the Ratchet is an important element of Brownian circuits, since it speeds up searching in circuits by restricting the movement of signals to one direction. Since searching is unable to backtrack over a ratchet, it will consume less time as a result. Use of the ratchet, however, should be carefully considered [8], as they cannot be placed in locations where they would interfere with the search process in the circuit.

Figure 8 shows the Half-Adder to which Ratchets are added. In the part of the circuit where signals need to search to find the CJoin matching the input to the circuit, no Ratchets

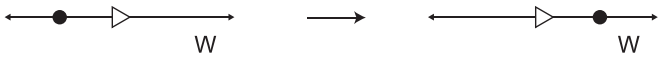

FIG. 7. Ratchet and its possible transition [8]. The token on the wire W may fluctuate before the ratchet as well as after the ratchet, but once it moves across the ratchet it cannot return. The ratchet thus imposes a direction on a (originally) bidirectional wire.

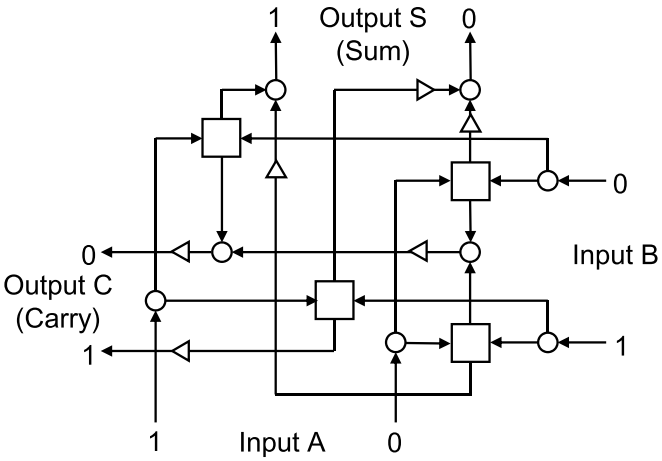

FIG. 8. Brownian circuit for a Half-Adder with Ratchets added. Ratchets are only placed at positions where they do not interfere with the random search.

are present to ensure that the circuit operates correctly. In other parts of the circuit, Ratchets can be employed freely, since restrictions to the random search process do not affect the circuit's operation. The energy consumption by Ratchets, however, may restrict their use. This motivates the use of the pseudoratchet effect emerging in 1D quantum Brownian motion as an energy-efficient alternative to conventional Ratchets.

APPENDIX C: TEMPERATURE DEPENDENCE OF NONZERO SOUND VELOCITY VIA PHONON QUANTUM STATISTICS

In this Appendix, we focus on the high-temperature condition under which the quantum-statistical distribution of phonons is approximated by a classical distribution, and qualitatively show that the sound velocity approaches zero under this condition.

Importantly, we emphasize that the high-temperature limit is conceptually distinct from the classical limit $\hbar \to 0$. In the classical limit, the collision operator itself vanishes, eliminating dissipation altogether, as noted below Eq. (11). In contrast, in the high-temperature regime, dissipation remains, but the asymmetry in transport diminishes as more discrete momenta in subspace become thermally populated and averaged out.

The Bose-Einstein distribution (11) indicates that lower-energy phonon modes are predominantly occupied at low temperatures, whereas higher-energy modes become increasingly populated as the temperature increases. In high-temperature regime,

$$\hbar\omega_q \ll k_B T, \tag{C1}$$

the distribution can be approximated by the classical Rayleigh-Jeans form,

$$n(q) \simeq \frac{k_B T}{\hbar\omega_q}, \tag{C2}$$

where virtually all phonon modes are thermally excited, and each mode carries an average energy of $k_B T$.

The high-temperature condition (C1) can be rewritten by substituting the phonon dispersion relation (5) as

$$c\hbar|q| \ll k_{\mathrm{B}}T. \tag{C3}$$

As explained in Sec. II A, the emission or absorption of a single phonon (carrying momentum $\hbar q$) leads to discrete momentum transitions of the particle in the 1D system. Due to momentum conservation and the resonance condition, the accessible discrete momenta P_ν form a subset (14).

In this framework, a single phonon-induced momentum transition is given by

$$\hbar|q| = |P_{\nu\pm1} - P_\nu|. \tag{C4}$$

Substituting this into the high-temperature condition (C3) and rearranging in terms of the momentum unit $p_{\mathrm{u}} = mc$ and temperature unit $T_{\mathrm{u}} = mc^2/k_{\mathrm{B}}$, we obtain

$$\frac{|P_{\nu\pm1} - P_\nu|}{p_{\mathrm{u}}} \ll \frac{T}{T_{\mathrm{u}}}. \tag{C5}$$

Under this condition, the phonon distribution approaches the classical form (C2), and phonons with larger momentum $\hbar|q|$ are thermally excited. As a result, the particle can undergo larger momentum transitions via phonon absorption and emission.

This behavior can be understood by examining the equilibrium momentum distribution of the particle, as shown in Fig. 9. We note that this figure is a revised version of the one presented in our previous work [34]. In addition to the original panels, we here added panel (c), which shows the equilibrium momentum distribution at a higher temperature $T = 5$. The comparison with $T = 1$ clearly highlights that the width of the Maxwellian momentum distribution expands, increasing the probability of transitions between states with larger momentum difference:

$$\Delta P_{\nu\pm1,\nu} := |P_{\nu\pm1} - P_\nu|. \tag{C6}$$

Consequently, a greater number of discrete momentum states are thermally excited. Note that the momentum difference $\Delta P_{\nu\pm1,\nu}$ corresponds to the transition between the dots connected by gray lines in Fig. 9(a), and does not represent the transition between adjacent discrete momentum states.

At a given temperature, the typical upper bound of momentum difference, $\Delta P_{\mathrm{upper}}$, can be roughly estimated by the width of the Maxwellian distribution:

$$\Delta P_{\mathrm{upper}} \sim 2\sqrt{mk_{\mathrm{B}}T}. \tag{C7}$$

Furthermore, the interval between two adjacent discrete momenta within a subspace can be expressed as

$$\delta P_{\nu,-(\nu\pm1)} := |P_\nu - P_{-(\nu\pm1)}| = 2|P_0 - mc|, \tag{C8}$$

where P_0 is the momentum satisfying $-mc \leqslant P_0 \leqslant mc$, leading to the following range:

$$0 \leqslant 2|P_0 - mc| \leqslant 4mc. \tag{C9}$$

Thus, the average interval is typically on the order of $\overline{\delta P} \sim 2mc$.

The number of discrete momentum states that are thermally excited at a given temperature can be estimated as

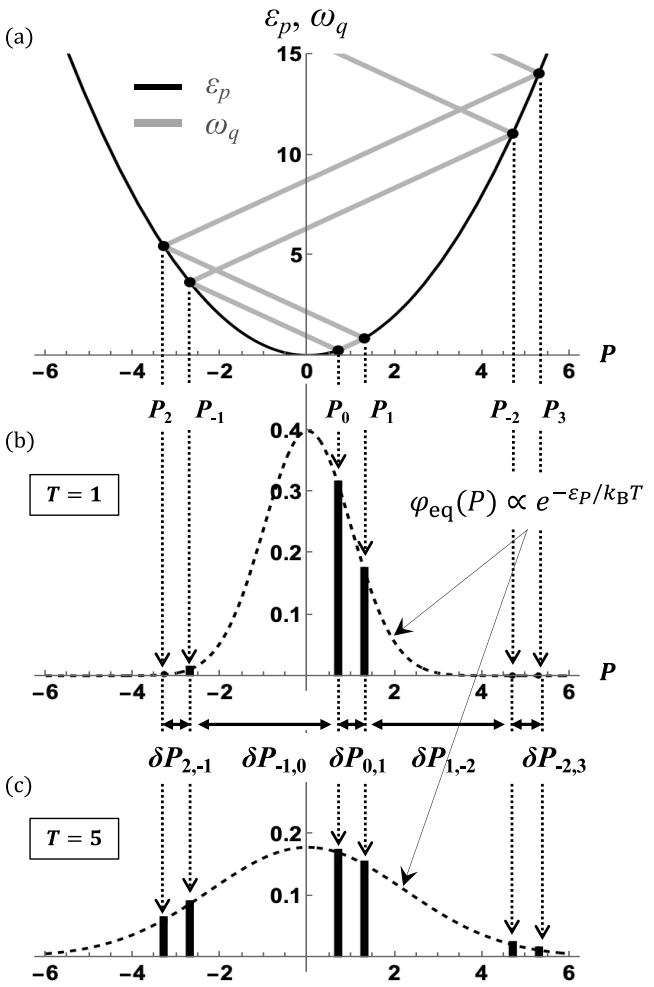

FIG. 9. Discrete momentum transitions in the 1D quantum system and the resulting asymmetric Maxwell distribution. All units are described as in the model introduction. (a) Discrete momentum subset accessible from $P_0 = 0.7$. (b) Momentum equilibrium distribution in the subspace $\mathcal{S}_{P_0=0.7}$ at $T = 1$ in the temperature unit T_{u}. Only a few momentum states near the origin are thermally excited. (c) Momentum equilibrium distribution in the same subspace at $T = 5$. A broader range of momentum states is excited.

follows:

$$\frac{\Delta P_{\mathrm{upper}}}{\overline{\delta P}} \sim \frac{2\sqrt{mk_{\mathrm{B}}T}}{2mc} = \sqrt{\frac{T}{T_{\mathrm{u}}}}. \tag{C10}$$

Accordingly, the system can be regarded as "low temperature" if this number is of order unity,

$$\sqrt{\frac{T}{T_{\mathrm{u}}}} \sim 1, \tag{C11}$$

and "high temperature" if this number is much greater than unity,

$$\sqrt{\frac{T}{T_{\mathrm{u}}}} \gg 1. \tag{C12}$$

This high-temperature condition, derived from the particle's momentum distribution, corresponds to the

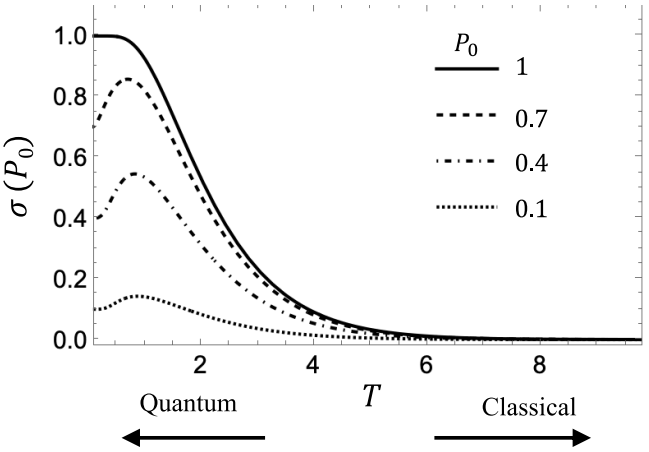

FIG. 10. Temperature dependence of the hydrodynamic sound velocity $\sigma(P_0)$. The units of temperature T_u and momentum p_u are those defined in Eq. (A1). The sound velocity is defined within each momentum subspace $\mathcal{S}_{P_0}$. The solid line corresponds to $P_0 = 1$, the dashed line to $P_0 = 0.7$, the dash-dotted line to $P_0 = 0.4$, and the dotted line to $P_0 = 0.1$. The sound velocity becomes large around $T \sim 1$ and asymptotically vanishes in the high-temperature regime $T \gg 1$.

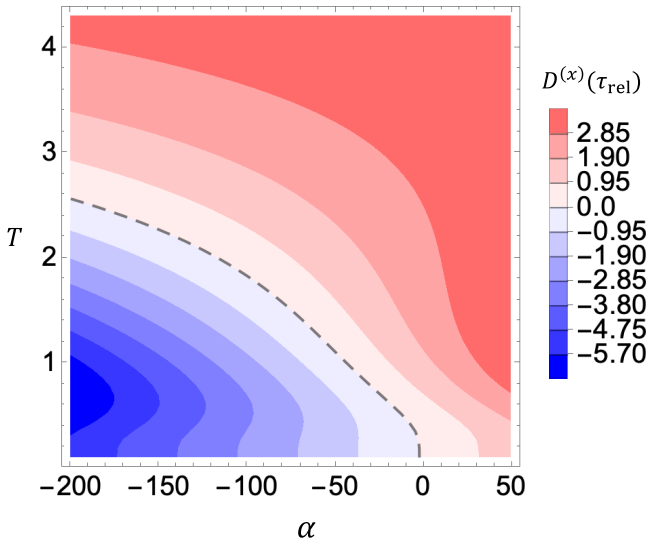

FIG. 11. Contour plot of $D^{(x)}(\tau_{\rm rel})$ for an initial nonfactorizable Gaussian wave packet (30), centered at $(X', P') = (0, 0)$ with width $\widetilde{\Delta X} = 3$. The dashed line shows the threshold at which the value becomes zero. This plot shows the α-T parameter region where the spatial contraction occurs. The values are computed using a parameter set representative of a protein molecular chain. In this setting, $D^*/D_u \sim 2$. All quantities are expressed in units introduced in Sec. II A: The unit of the diffusion coefficient is $D_u = x_u^2/t_u \sim 6 \times 10^{-3}$ cm^2/s, the unit of temperature is $T_u \sim 200$ K, and the unit of the initial shift parameter α is $x_u/p_u = \hbar/m^2c^2 \sim 2 \times 10^{14}$ s/kg, with the effective mass $m \simeq 2 \times 10^{-28}$ kg, and the acoustic phonon propagation speed $c \simeq 4000$ m/s. The large unit value of α is due to the small effective mass of the molecular system.

phonon-based high-temperature condition (C5) when the representative momentum transition is set to

$$|P_{\nu\pm1} - P_\nu| \sim mc. \tag{C13}$$

Here, mc corresponds to half of the average interval $\overline{\delta P} \sim 2mc$ between adjacent discrete momentum states. When the temperature is on the order of mc, only one or two discrete momentum states that are very close together (i.e., with the same sign) are thermally excited, as shown in Fig. 9(b). Consequently, the contributions from positive and negative momenta do not cancel out, and the sound velocity remains nonzero. Therefore, both conditions are qualitatively consistent: Increasing the temperature leads to the thermal excitation of more phonon modes with larger momentum, thereby allowing the particle to access a broader range of momentum states.

Now, let us focus on the temperature dependence of the sound velocity (21). The sound velocity is defined as the average momentum in units in which $m = 1$, weighted by the Maxwellian momentum distribution over the discrete momentum states within the subspace $\mathcal{S}_{P_0}$.

Figure 10 reproduces the temperature dependence of the sound velocity $\sigma(P_0)$ that we previously reported in Ref. [29]. We include it here again as a convenient reference for comparison between the high-temperature condition (C12) and the temperature range where unidirectional transport becomes prominent.

At low temperatures, only a few discrete momentum states near the origin are significantly populated. Due to the inversion asymmetry of the subspace $\mathcal{S}_{P_0}$, their contributions to the sound velocity do not cancel out, resulting in a nonzero value. As the temperature increases, however, a broader range of momentum states becomes thermally excited. As a result, the positive and negative momentum contributions become more balanced, leading to cancellation in the average, and the sound velocity gradually decreases toward zero. This behavior is illustrated in Fig. 10.

In the high-temperature regime (C12), i.e., $T/T_u \gg 1$, the sound velocity asymptotically approaches zero, as shown in Fig. 10. Thus, in this regime, the particle behaves similarly to the phenomenologically hypothesized 1D classical Brownian motion, in which no unidirectional transport occurs.

In summary, the characteristic temperature T_u defined as a unit temperature characterizes the quantum-to-classical crossover in this system. This crossover is distinct from the behavior in the classical limit $\hbar \to 0$, as discussed at the beginning of this Appendix.

APPENDIX D: THRESHOLD TEMPERATURE FOR THE SPATIAL CONTRACTION

In this Appendix, we identify the threshold temperature below which the system, with the initial distribution (30), exhibits spatial contraction.

For this analysis, we adopt parameter values relevant to the α-helical protein molecular chain [40,49]. This choice is motivated by the fact that, in the protein molecular chain, the ratchet effect remains observable at temperatures on the order of 10^2 K, while for semiconductor parameters, it becomes significant only at much lower temperatures on the order of 10^{-1} K.

In α-helical protein molecular chain system, the characteristic scale of the diffusion coefficient (A2) is estimated as $D^* \sim 0.01\ \mathrm{cm}^2/\mathrm{s}$, with the deformation potential $\Delta_0 \simeq 0.3$ eV and the 1D mass density $\rho_M \simeq 1 \times 10^{-15}$ kg/m. Note that under these parameters, the ratio between the characteristic diffusion scale and the diffusion unit is approximately $D^*/D_{\mathrm{u}} \sim 2$.

As discussed in Sec. III, the spatial contraction can be observed during the time interval (51). For such a time interval to exist, the inequality $\tau_{\mathrm{rel}} < t_d$ must be satisfied. Using Eq. (48), this inequality can be rewritten as

$$D^{(x)}(\tau_{\mathrm{rel}}) < 0. \tag{D1}$$

By varying the temperature T and initial shift parameter α and plotting $D^{(x)}(\tau_{\mathrm{rel}})$, we obtain a contour plot as shown in Fig. 11. The bottom-left (blue) region represents the parameter space where $D^{(x)}(\tau_{\mathrm{rel}}) < 0$, indicating that the advection effect dominates over diffusion and the system exhibits spatial contraction. The dashed contour line corresponds to the threshold where $D^{(x)}(\tau_{\mathrm{rel}}) = 0$. In the top-right (red) region above this line, the diffusion dominates and the system does not exhibit spatial contraction.

As estimated in the concluding remarks, room temperature, 300 K, corresponds to $T/T_{\mathrm{u}} = 1.5$ under the protein parameters. Even at such relatively high temperatures, the advection effect can still dominate over the diffusion effect, and spatial contraction can occur.

[1] C. H. Bennett, The thermodynamics of computation—A review, Int. J. Theor. Phys. **21**, 905 (1982).

[2] C. H. Bennett, Logical reversibility of computation, IBM J. Res. Dev. **17**, 525 (1973).

[3] R. P. Feynman, Quantum mechanical computers, Found. Phys. **16**, 507 (1986).

[4] T. Toffoli, Reversible computing, in *International Colloquium on Automata, Languages, and Programming* (Springer, Berlin, 1980), pp. 632–644.

[5] E. Fredkin and T. Toffoli, Conservative logic, Int. J. Theor. Phys. **21**, 219 (1982).

[6] R. Landauer, Irreversibility and heat generation in the computing process, IBM J. Res. Dev. **5**, 183 (1961).

[7] P. Strasberg, J. Cerrillo, G. Schaller, and T. Brandes, Thermodynamics of stochastic Turing machines, Phys. Rev. E **92**, 042104 (2015).

[8] J. Lee and F. Peper, On Brownian cellular automata, in *Automata* (Luniver Press, Frome, UK, 2008), pp. 278–291.

[9] F. Peper, J. Lee, J. Carmona, J. Cortadella, and K. Morita, Brownian circuits: Fundamentals, ACM J. Emerging Technol. Comput. Syst. **9**, 1 (Luniver Press, Frome, United Kingdom, 2013).

[10] J. Lee, F. Peper, S. D. Cotofana, M. Naruse, M. Ohtsu, T. Kawazoe, Y. Takahashi, T. Shimokawa, L. B. Kish, and T. Kubota, Brownian circuits: Designs, Int. J. Unconv. Comput. **12**, 341 (2016).

[11] I. Ercan and E. Suyabatmaz, Fundamental energy limits of SET-based Brownian NAND and half-adder circuits, Eur. Phys. J. B **91**, 113 (2018).

[12] I. Ercan, Z. D. Sütgöl, and F. O. Özhan, Physical limitations on fundamental efficiency of set-based brownian circuits, Entropy **23**, 406 (2021).

[13] Y. Jibiki, M. Goto, E. Tamura, J. Cho, S. Miki, R. Ishikawa, and Y. Suzuki, Skyrmion brownian circuit implemented in continuous ferromagnetic thin film, Appl. Phys. Lett. **117**, 082402 (2020).

[14] M. A. Brems, M. Kläui, and P. Virnau, Circuits and excitations to enable Brownian token-based computing with skyrmions, Appl. Phys. Lett. **119**, 132405 (2021).

[15] S. Kawakami, Y. Ohtsubo, K. Inoue, and M. Tanaka, Late breaking results: Single flux quantum based brownian circuits for ultra-low-power computing, in *2024 Design, Automation & Test in Europe Conference & Exhibition (DATE)* (Valencia, Spain, 2024), pp. 1–2.

[16] J. D. Norton, Brownian computation is thermodynamically irreversible, Found. Phys. **43**, 1384 (2013).

[17] K. J. Ray, A. B. Boyd, G. W. Wimsatt, and J. P. Crutchfield, Non-Markovian momentum computing: Thermodynamically efficient and computation universal, Phys. Rev. Res. **3**, 023164 (2021).

[18] J. A. Owen, A. Kolchinsky, and D. H. Wolpert, Number of hidden states needed to physically implement a given conditional distribution, New J. Phys. **21**, 013022 (2019).

[19] E. Stopnitzky, S. Still, T. E. Ouldridge, and L. Altenberg, Physical limitations of work extraction from temporal correlations, Phys. Rev. E **99**, 042115 (2019).

[20] A. Pal, S. Reuveni, and S. Rahav, Thermodynamic uncertainty relation for first-passage times on Markov chains, Phys. Rev. Res. **3**, L032034 (2021).

[21] U. Seifert, Stochastic thermodynamics, fluctuation theorems and molecular machines, Rep. Prog. Phys. **75**, 126001 (2012).

[22] Y. Utsumi, Y. Ito, D. Golubev, and F. Peper, Computation time and thermodynamic uncertainty relation of brownian circuits, arXiv:2205.10735.

[23] Y. Utsumi, D. Golubev, and F. Peper, Thermodynamic cost of Brownian computers in the stochastic thermodynamics of resetting, Eur. Phys. J. Spec. Top. **232**, 3259 (2023).

[24] H. Risken, Fokker-Planck equation for several variables; methods of solution, in *The Fokker-Planck Equation: Methods of Solution and Applications* (Springer, Heidelberg, 1996), pp. 133–162.

[25] M. O. Magnasco, Forced thermal ratchets, Phys. Rev. Lett. **71**, 1477 (1993).

[26] R. D. Astumian and M. Bier, Fluctuation driven ratchets: Molecular motors, Phys. Rev. Lett. **72**, 1766 (1994).

[27] R. D. Astumian, Thermodynamics and kinetics of a Brownian motor, Science **276**, 917 (1997).

[28] P. Reimann, Brownian motors: Noisy transport far from equilibrium, Phys. Rep. **361**, 57 (2002).

[29] S. Nakade, K. Kanki, S. Tanaka, and T. Petrosky, Anomalous diffusion of a quantum Brownian particle in a one-dimensional molecular chain, Phys. Rev. E **102**, 032137 (2020).

[30] R. P. Feynman, R. B. Leighton, and M. Sands, *The Feynman Lectures on Physics* (Addison-Wesley, Reading, MA, 1963), Vol. 1.

[31] L. Szilard, On the decrease of entropy in a thermodynamic system by the intervention of intelligent beings, Behav. Sci. **9**, 301 (1964).

[32] T. Sagawa, Second law, entropy production, and reversibility in thermodynamics of information, in *Energy Limits in Computation: A Review of Landauer's Principle, Theory and Experiments* (Springer, Berlin, 2018), pp. 101–139.

[33] S. Nakade, K. Kanki, S. Tanaka, and T. Petrosky, Anomalous diffusion with an apparently negative diffusion coefficient in a one-dimensional quantum molecular chain model, Symmetry **13**, 506 (2021).

[34] S. Tanaka, K. Kanki, and T. Petrosky, Emergence of quantum hydrodynamic sound mode of a quantum Brownian particle in a one-dimensional molecular chain, Phys. Rev. B **80**, 094304 (2009).

[35] T. Petrosky, N. Hatano, K. Kanki, and S. Tanaka, Hofstadter's butterfly type of singular spectrum of a collision operator for a model of molecular chains, Prog. Theor. Phys. Suppl. **184**, 457 (2010).

[36] P. Résibois and M. de Leener, *Classical Kinetic Theory of Fluids* (John Wiley & Sons, New York, 1977).

[37] T. M. Cover, *Elements of Information Theory* (John Wiley & Sons, New York, 1999).

[38] I. Prigogine, *Nonequilibrium Statistical Mechanics* (John Willey & Sons, New York, 1962).

[39] A. S. Davydov, Solitons in quasi-one-dimensional molecular structures, Sov. Phys. Usp. **25**, 898 (1982).

[40] A. Scott, Davydov's soliton, Phys. Rep. **217**, 1 (1992).

[41] G. D. Mahan, *Many-Particle Physics*, 2nd ed. (Plenum, New York and London, 2013).

[42] T. Petrosky and I. Prigogine, The Liouville space extension of quantum mechanics, Adv. Chem. Phys. **99**, 1 (1997).

[43] T. Petrosky and I. Prigogine, Poincaré resonances and the extension of classical dynamics, Chaos, Solitons Fractals **7**, 441 (1996).

[44] R. L. Hudson, When is the Wigner quasi-probability density non-negative? Rep. Math. Phys. **6**, 249 (1974).

[45] U. Leonhardt and H. Paul, Measuring the quantum state of light, Prog. Quantum Electron. **19**, 89 (1995).

[46] C. E. Shannon, A mathematical theory of communication, Bell Syst. Tech. J. **27**, 379 (1948).

[47] A. B. Boyd, D. Mandal, and J. P. Crutchfield, Identifying functional thermodynamics in autonomous Maxwellian ratchets, New J. Phys. **18**, 023049 (2016).

[48] R. Sánchez, P. Samuelsson, and P. P. Potts, Autonomous conversion of information to work in quantum dots, Phys. Rev. Res. **1**, 033066 (2019).

[49] P. L. Christiansen and A. C. Scott, *Davydov's Soliton Revisited: Self-Trapping of Vibrational Energy in Protein* (Plenum, New York, 1990).

[50] K. J. Ray and J. P. Crutchfield, Gigahertz sub-Landauer momentum computing, Phys. Rev. Appl. **19**, 014049 (2023).